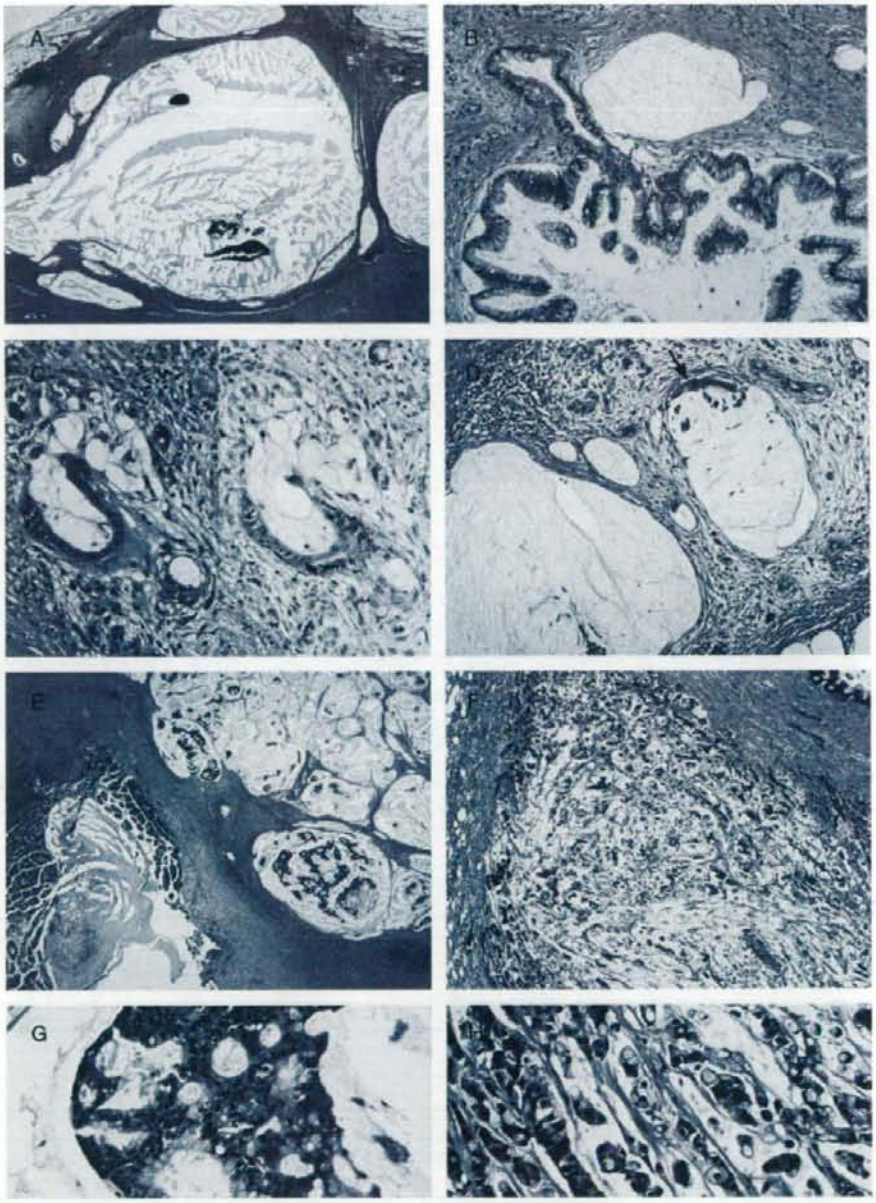

FIGURE 2. Histopathologic features of "mucous rupture" and "infiltrative growth" of mucinous carcinoma in I-IPMC. A to D, "Mucous rupture" pattern. Part of the pancreatic duct is disrupted and mucus leakage is evident. Variable sizes of mucus lakes without viable cancer cells floating are observed (A–C). A small duct covered by elastic fibers (C right column; elastica stain) is broken and the mucus leaks to form mucus lake (C). A small number of cancer cells (arrow) are floating in mucus lakes, which is described as "mucous rupture with cellular component." We could not observe any floating cancer cells in mucus lakes other than this cluster of cancer cells (arrow) in the entire lesion of the I-IPMC (D). E to H, "Infiltrative growth" of mucinous carcinoma. Many cancer cells floating in mucus lakes (E, G) or infiltrating features of mucinous carcinoma (F, H) are categorized as "infiltrative growth" of mucinous carcinoma. G and H, High-power view of (E) and (F), respectively.

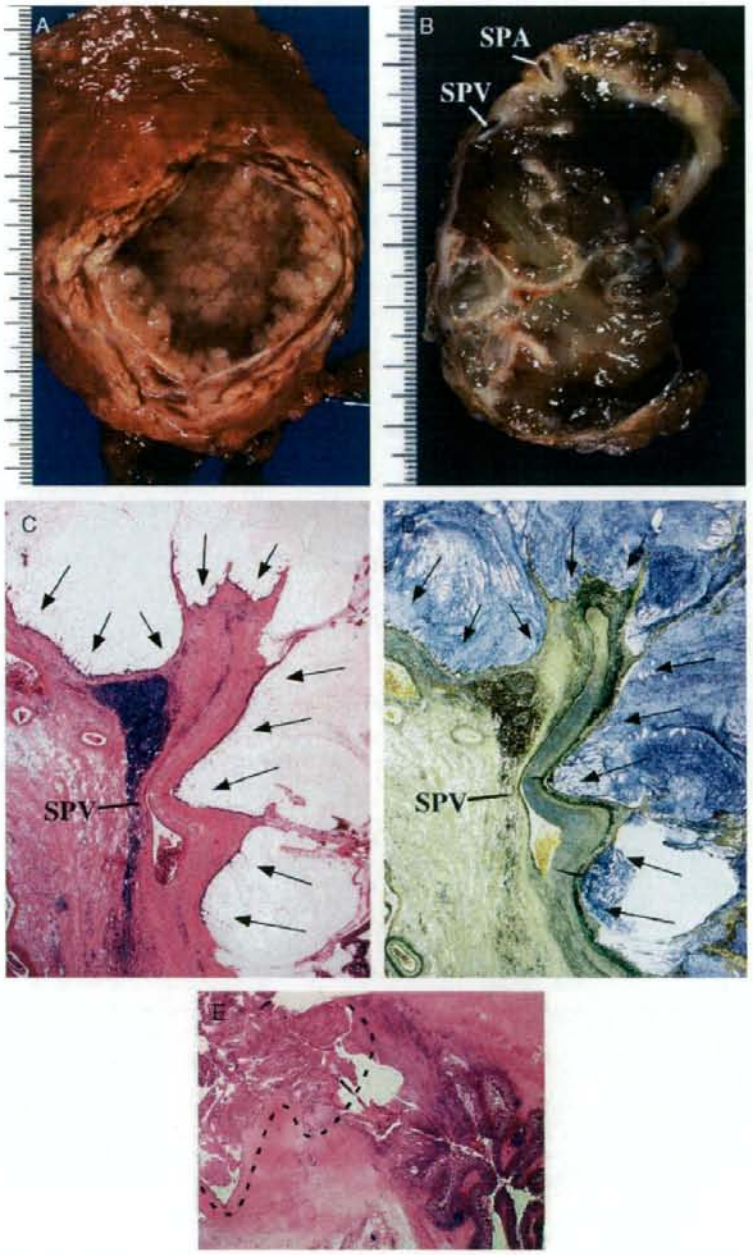

FIGURE 3. Histopathologic features of "expansive growth" in I-IPMC. The pancreatic duct is markedly dilated to a cystlike shape (A, B). Fresh cut view (A) and formalin-fixed cut surface (B) of cystic I-IPMCs. Cystically dilated pancreatic duct is filled with clear mucus and many papillary projections are seen on the inner surface (A). The SPV is compressed (B–D) and its thickened wall is eroded by an enlarged cystic IPMC (arrows) in hematoxylin and eosin stain (C) and elastica stain (D). A fistula has been formed between cystic I-IPMC (dotted line) and duodenum (E).

All of the 24 patients with mucous rupture MI-IPMC survived after surgery.

Expansive growth of ductectatic or cystic IPMN is another characteristic feature of IPMN (Fig. 3). In addition to mucous rupture, an increase of intraductal pressure by hypersecretion of mucus causes marked cystic dilatation of the duct, which continues to grow expansively into extrapancreatic tissue. In some cases, cystic IPMC eventually forms a fistula with surrounding digestive organs (Fig. 3E) or erodes the wall of major blood vessels [portal vein, splenic vein (SPV), superior mesenteric vein (SMV), or splenic artery] (Figs. 3C–E). Such growth and spread are rather passive in contrast to the infiltrative growth that occurs in active invasion and this feature was not associated with poor prognosis, similarly to mucous rupture. IPMC showing expansive growth with loss of the basement membrane of the pancreatic duct in the IPMC is diagnosed as MI-IPMC. If I-IPMC grows expansively, even if it ruptures into the bowel, or even if it erodes a major vessel wall unless cancer cells enter the lumen of the major vessel, it is still regarded as minimal invasion (Table 1). If I-IPMC has this type of growth as predominance, it is corresponded to a kind of pure mucinous carcinoma associated with IPMC.

Although we have not yet experienced intra-abdominal rupture of IPMC, a few cases have been reported.[18] As intra-abdominal rupture was followed by peritoneal dissemination in these reported cases, this type should be distinguished from ordinary IPMN and managed separately as ruptured IPMN.

IC-IPMC was defined as a lesion consisting of IPMN and invasive carcinoma with the predominance of the IPMN component.[12] Such invasive carcinoma exceeds the minimal invasion proposed in Table 1, and shows a continuous transition between invasive carcinoma and intraductal IPMC. In this study, we added new group of cases to the original IC-IPMC category, which had invasive carcinoma apparently originated from IPMN but predominant over the IPMN component. We wanted to compare the prognosis between IC-IPMC and conventional invasive ductal carcinoma of the pancreas in the matched tumor-node-metastasis (TNM) stages.[11]

Statistical Analysis

Comparisons of qualitative variables were performed using the χ^2 test or Fisher exact test. One-way analysis of variance was used to compare the means of 3 or more groups. The postoperative overall and disease-specific survival rates were calculated by the Kaplan-Meier method. Univariate analysis was performed for prognostic factors using the log-rank test. The factors found to be predictive by univariate analysis were subjected to multivariate analysis using the Cox proportional hazards model. Differences at $P < 0.05$ were considered statistically significant. Statistical analyses were performed with SPSS 11.0J software (SPSS Inc, Chicago, IL).

RESULTS

Histopathologic Evaluation of I-IPMC

One hundred and four IPMNs were classified into 27 IPMAs, 11 borderline IPMNs, 15 noninvasive IPMCs, and 51 I-IPMCs according to the WHO classification.[13,15] None of them had an ovarianlike stroma, and all the lesions showed communication with the pancreatic ductal system. I-IPMCs were further divided into 26 MI-IPMCs and 25 IC-IPMCs according to our criteria (Table 1) based on the histopathologic pattern of invasion.

To evaluate the aggressive characteristics of I-IPMC, we examined the invasiveness of I-IPMC. The invasiveness was categorized into 4 patterns: infiltrative growth, mucous rupture, expansive growth, and intra-abdominal rupture (see Materials and Methods). The criterion of minimal invasion was proposed for each corresponding pattern (Table 1), and the representative features are shown in Figures 1 to 3.

Seventeen among 26 patients with MI-IPMC showed infiltrative growth pattern (Fig. 1). Histologic types of the infiltrating cancer cells were tubular adenocarcinoma in 7 patients, mixed tubular adenocarcinoma and mucinous carcinoma in 2 patients, pure mucinous carcinoma in 5 patients, and papillary adenocarcinoma in 3 patients. The average depth of infiltration was 1.5 mm (range from < 1 to 5 mm). None of the 17 patients with a maximum infiltration of 5 mm or less had recurrence with exception of 2 patients, one of them had 2-mm-length infiltration of tubular adenocarcinoma and the other had 2-mm-length infiltration of pure mucinous carcinoma.

The most of the patients with MI-IPMC had mucous rupture and 6 patients had MI-IPMC with mucous rupture as predominant invasive pattern (Fig. 2). Two of them were subcategorized as mucous rupture with cellular component. None of these 6 patients had recurrence.

Expansive growth (Fig. 3) was often observed in cystically growing tumors and 4 patients with MI-IPMC mentioned below showed expansive growth as predominance. In 2 patients with I-IPMC, a fistula was formed between the IPMN and the duodenum. No cancer cells infiltrating the duodenal wall were detected in either case by histologic examination (Fig. 3E). It was suspected that the fistulas were formed by rupture of the expansively growing IPMN into the adjacent duodenum. The lesion was classified as MI-IPMC (expansive growth) in 1 patient, but the other patient had definite invasive cancer in the pancreas tail distant from the fistula, and was therefore diagnosed as having IC-IPMC. Whereas the former patient had no recurrence 107 months after surgery, the latter patient developed local lymph node (LN) metastasis 6 months after surgery and died of the disease. In the other 3 patients with expansive growth of MI-IPMC, the IPMN had grown deeply into the retropancreatic tissue, compressing the wall of the SPV or SMV. In one of them, the tunica media of the SPV was involved without a fistula

TABLE 2. Comparison of Invasive Lesion Between MI-IPMC and IC-IPMC

	MI-IPMC (n = 26)	IC-IPMC (n = 25)	P*
Growth pattern			
Infiltrative growth	17	25	
Mucous rupture or expansive growth as predominance	10†	0	
Vessel or neural invasion	4	25	**< 0.001**
Lymphatic invasion	0	23	**< 0.001**
Venous invasion	2	24	**< 0.001**
Intrapancreatic neural invasion	2	22	**< 0.001**
Extrapancreatic involvement	4	23	**< 0.001**
Serosa	0	4	0.051
Retropancreatic tissue	3‡	21	**< 0.001**
Duodenum	1‡	8	**0.002**
Extrahepatic bile duct	0	3	0.110
Portal venous system	1‡	8	**0.011**
Arterial system	0	1	0.490
Extrapancreatic nerve plexus	0	4	0.051
Invasion to surgical margin	0	4	0.051
Metastasis	0	17	**< 0.001**
Local LN	0	17	**< 0.001**
Distant organs	0	4§	0.051
TNM stage			**< 0.001**
IA	22	1	
IB	0	0	
IIA	4	7	
IIB	0	13	
III	0	0	
IV	0	4§	
Histology of infiltrative growth			
Pap	3	2	
Tub1	7	5	
Tub2	0	8	
Tub + Muc	2	7	
Tub3	0	1	
Muc	5	1	
AS	0	1	

Statistically significant value is in bold characters.

*P value was calculated by χ^2 or Fisher exact test.

†6 patients showed mucous rupture (2 of them showed mucous rupture with cellular component) and 4 patients showed expansive growth (one of them showed infiltrative growth as well).

‡Due to expansive growth.

§One patient with liver metastasis, 3 patients with para-aortic LN metastasis.

AS indicates adenosquamous carcinoma; Muc, mucinous carcinoma; Pap, papillary adenocarcinoma; Tub1, well-differentiated tubular adenocarcinoma; Tub2, moderately differentiated tubular adenocarcinoma; Tub3, poorly differentiated tubular adenocarcinoma.

between tumor and SPV (Figs. 3C–E). These 3 patients did not have postoperative recurrence at 28, 52, and 96 months after surgery, respectively. We thought mucous rupture and expansive growth is dormant invasion, considering its nonaggressive nature, which is characteristic to IPMN.

Comparison of the pathologic characteristics and TNM staging[11] between invasive lesions of MI-IPMCs and IC-IPMCs are summarized in Table 2. Vessel or neural invasion and extrapancreatic involvement were much more common in IC-IPMC than in MI-IPMC. No LN metastasis was observed in patients with MI-IPMC, whereas 17 patients (68%) with IC-IPMC showed LN metastasis. With regard to the histology of the invasive component of the IC-IPMC, most of the patients had tubular adenocarcinoma and only 1 patient had pure mucinous carcinoma. Among 26 patients with MI-IPMC, 9 had tubular adenocarcinoma and 11 had pure mucinous carcinoma.

Prognostic Significance of the Classification of I-IPMC

The median survival period for the 104 patients was 142 months, and the 3, 5, and 10-year overall survival rates were 86%, 78%, and 59%, respectively. There was no statistically significant difference in overall survival among patients with IPMA, borderline IPMN, and noninvasive IPMC ($P = 0.54$). Therefore, they were integrated into noninvasive IPMN for subsequent analysis. The survival rates 3, 5, and 10 years after surgery were 95%, 92%, and 70% for noninvasive IPMN, 95%, 79%, and 79% for MI-IPMC, and 51%, 38%, and 0% for IC-IPMC (Fig. 4A). The disease-specific survival rates after 3, 5, and 10 years were 100%, 100%, and 100% for noninvasive IPMN, 100%, 100%, and 100% for MI-IPMC, and 51%, 38%, and 0% for IC-IPMC (Fig. 4B). Overall and disease-specific survival for MI-IPMC was significantly better than for IC-IPMC ($P < 0.001$), whereas there was no significant difference in overall survival between noninvasive IPMN and MI-IPMC ($P = 0.66$).

Overall survival was compared between I-IPMC and conventional invasive ductal carcinoma of the pancreas during the same period (Figs. 5A–D). The stages of IC-IPMCs were assessed on the basis of size and spread of invasive carcinoma in the lesion, using the International Union against Cancer (UICC) TNM classification,[11] and classified as stage IA, IB, and IIA, stage IIB, and stage III and IV. Between IC-IPMC and conventional invasive ductal carcinoma of the pancreas at each corresponding TNM stage, there was no statistically significant difference in survival rate, though IC-IPMC had a tendency to show a favorable outcome.

Prognostic Factors in I-IPMCs

Clinicopathologic factors possibly affecting the postoperative outcome of I-IPMCs were studied (Table 3). The following variables were significantly related to unfavorable prognosis: presence of jaundice, cancer cells present at the surgical margin except the pancreatic margin, presence of major vascular invasion [portal vein, SMV, SPV, or splenic artery], presence of lymphatic invasion, presence of venous invasion, presence of intrapancreatic neural invasion, presence of LN metastasis, presence of para-aortic LN metastasis, CA19-9 > 300 U/mL, size of invasive cancer > 2 cm, histopathologic diagnosis of IC-IPMC (vs. MI-IPMC), and tubular adenocarcinoma as histologic type of invasive cancer in I-IPMC. Multivariate analysis (backward elimination method) showed that a histopathologic diagnosis of I-IPMC classified as IC-IPMC and

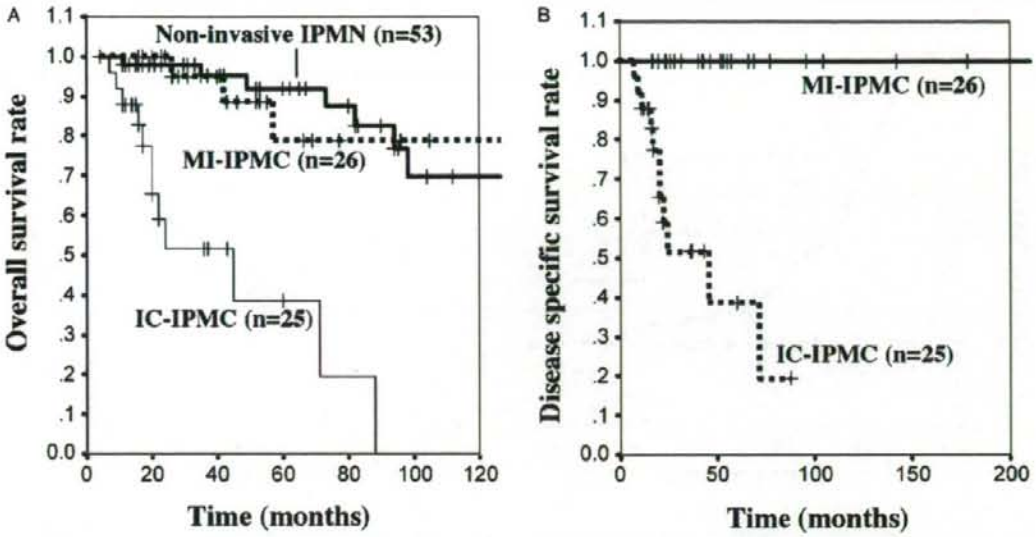

FIGURE 4. Kaplan-Meier survival curves of the 104 patients with IPMNs. A, Overall survival of patients with MI-IPMC was significantly better than that of patients with IC-IPMC ($P<0.001$), whereas no significant difference was found between patients with noninvasive IPMN and those with MI-IPMC ($P=0.66$). B, Disease-specific survival of patients with MI-IPMC was significantly better than that of patients with IC-IPMC ($P<0.001$), with no disease-related death among 26 patients with MI-IPMC during a median follow-up period of 43.4 (13.2 to 210) months.

CA19-9 > 300 U/mL were significant prognostic factors (Table 4).

Postoperative Recurrence of IPMNs

Postoperative recurrence was observed in 15 patients exclusively among those with I-IPMC (Table 5). Two patients with MI-IPMC suffered recurrence of MI-IPMC and invasive cancer in the remnant pancreas 36 and 48 months after surgery, respectively. At initial surgery, both patients had undergone PPPD for IPMNs in the pancreas head with negative surgical margins. The former underwent completion pancreatectomy in a second operation, and pathologic examination revealed another MI-IPMC in the remnant pancreas distant from the site of pancreato-jejunostomy. In the latter patient, recurrence of invasive ductal carcinoma was also found distant from the pancreato-jejunostomy, and additional partial resection of the remnant pancreas was performed. Both patients are currently doing well with no evidence of recurrence 8 and 20 months after the second operation, respectively. The remaining 13 recurrences were observed in patients with IC-IPMC. The site of recurrence was local (remnant pancreas) in 2 patients, LN in 2 patients, the lung in 1 patient, the liver in 4 patients, and peritoneal dissemination in 4 patients (Table 5). The time interval between surgery and recurrence was less than 20 months in all cases, with an especially short duration of 6.15 ± 0.82 months for patients with peritoneal dissemination.

Analysis of the Pancreatic Surgical Margin

Intraoperative frozen section analysis of the pancreas margin was performed in 96 patients, and 17 patients needed additional pancreatic resection owing to the confirmed or suspected presence of cancer cells at the pancreatic surgical margin (Table 5). Additional resection was performed more frequently in patients with MI-IPMC and IC-IPMC than in those with noninvasive IPMN, regardless of IPMN size ($P = 0.007$). The final pancreatic margin status was negative in 75 patients, positive for IPMA in 25, borderline IPMN in 2, noninvasive IPMC in 1, and invasive carcinoma in 1.

DISCUSSION

Many groups have investigated the malignant potential of IPMNs,[4,6,16,20,22–24] and the recent consensus is that its aggressiveness is dependent on the presence of invasive cancer, the extent of cancer invasion, and the biologic characteristics of the cancer cells.[2,3,8,10,14,15] However, no sufficient pathologic and presurgical staging system has yet been established for evaluating the malignant potential of I-IPMC. In this study, we examined 104 IPMNs surgically resected at the same hospital and proposed histopathologic criteria for classification of I-IPMC. I-IPMC shows heterogeneous features, which reflect the presence of heterogeneous cancer types with different biologic behaviors. Therefore, the criteria of MI-IPMC should differ in accordance with each histopathologic pattern of invasion. Our proposed

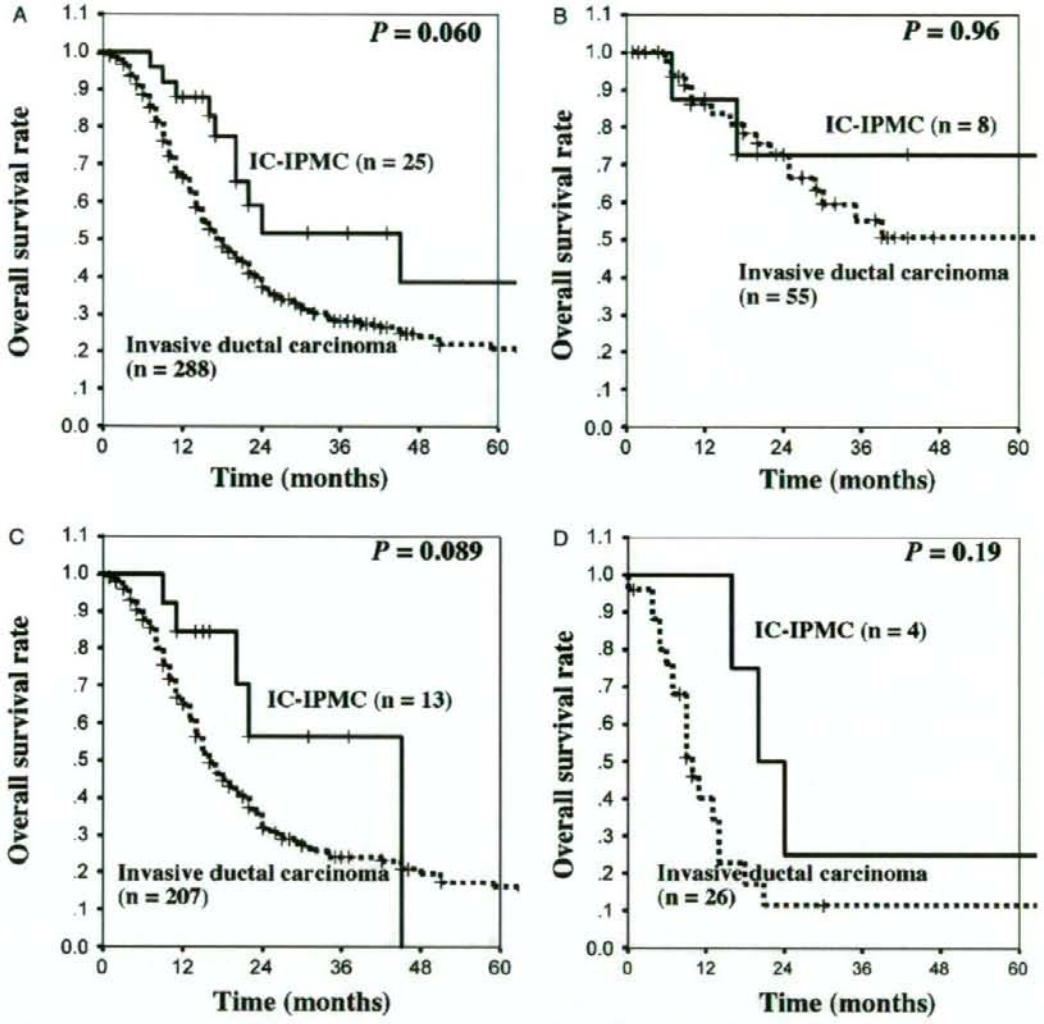

FIGURE 5. Kaplan-Meier survival curves of the 25 patients with IC-IPMC and the 288 patients with invasive ductal carcinoma of the pancreas. Comparison of overall survival of the patients with IC-IPMC and that of patients with conventional invasive ductal carcinoma at all stages (A), and in stage IA, IB, and IIA (B), stage IIB (C), and stage III and IV (D). Although the patients with IC-IPMC tended to have a better outcome than those with conventional invasive ductal carcinoma at each corresponding stage, the difference was not statistically significant.

criteria of invasiveness were successful in categorizing IPMCs in our series into noninvasive IPMC, MI-IPMC, and IC-IPMC. Patients with IC-IPMC had a significantly worse outcome than those with MI-IPMC. However, there was no difference in postoperative outcome between patients with MI-IPMC and those with noninvasive IPMC. This is the first report to propose practical criteria for MI-IPMC that can separate early-stage nonaggressive I-IPMC from total I-IPMC. Discrimination between MI-IPMC and IC-IPMC can provide important information for predicting the postoperative outcome of patients with IPMNs and also for deciding additional clinical management.

When IC-IPMCs were staged according to the size and spread of an invasive carcinoma component, the survival curve showed a similar decline to that of conventional invasive ductal carcinomas of the corresponding TNM stage, suggesting that it is the invasive

TABLE 3. Prognositic Factors of I-IPMCs in Univariate Analysis

Variables	n	Survival Rate 1y	3y	5y	P (Log-rank Test)
Sex					0.262
M	27	96.3	80.4	80.4	
F	24	91.7	70.4	41.5	
Age (y)					0.082
≤70	33	100.0	80.6	72.6	
>70	18	83.3	67.3	46.2	
Tumor location					0.937
Ph included	33	93.9	72.4	60.8	
Ph excluded	18	94.4	84.0	67.2	
Tumor distribution					0.821
Confined in 1 segment	35	91.4	75.7	63.2	
Diffuse (≥2 segments)	16	100.0	76.6	63.8	
PV resection					0.471
+	5	80.0	53.3	53.3	
−	46	95.7	78.0	63.0	
Chief complaint*					0.225
+	28	92.9	65.6	49.2	
−	23	95.6	90.0	81.0	
Jaundice					**0.011**
+	6	83.3	27.8	0.0	
−	45	95.6	80.7	66.2	
IPMN type					0.571
MPD or mixed	40	97.5	76.2	59.0	
BD	11	81.8	72.7	72.7	
MPD diameter					0.422
≤8 mm	31	90.3	75.4	52.2	
>8 mm	20	100.0	75.6	75.6	
Additional resection of pancreas†					0.864
+	14	92.9	63.7	63.7	
−	37	94.6	78.4	60.3	
Surgical margin (except for pancreas margin)‡					**<0.001**
+ or ±	4	75.0	0.0	0.0	
−	47	95.7	84.4	69.1	
Major vascular invasion (SMV, SPV, PV, or SPA)					**0.009**
+	10	90.0	48.2	0.0	
−	41	95.1	82.0	71.2	
Lymphatic invasion					**<0.001**
+	23	87.0	44.7	22.4	
−	28	100.0	95.5	81.7	
Venous invasion					**0.006**
+	26	88.5	53.5	42.8	
−	25	100.0	94.4	78.0	
Intrapancreatic neural invasion					**<0.001**
+	24	87.5	52.7	39.5	
−	27	100.0	94.4	78.4	
Local LN metastasis					**<0.001**
+	18	88.9	47.1	23.5	
−	33	97.0	88.9	76.4	
Para-aortic LN metastasis					**<0.001**
+	3	100.0	0.0	0.0	
−	48	93.8	32.3	67.4	
CEA (ng/mL)					0.455
≤5	35	94.3	83.4	64.3	
>5	16	93.8	58.4	58.4	
CA19-9 (U/mL)					**<0.001**
≤300	40	97.5	84.5	79.8	
>300	11	81.8	40.9	0.0	
IPMN size (mm)					0.552
≤40	15	93.3	70.2	43.9	
>40	36	94.4	78.2	72.2	
IPMN size (mm)					0.762
≤70	33	90.9	74.8	60.0	
>70	18	100.0	77.0	66.0	
Size of invasive lesion (mm)					0.001
≤20	32	96.9	88.7	75.1	
>20	19	89.5	48.7	32.4	
Pathologic diagnosis					**<0.001**
MI-IPMC	26	100.0	94.7	78.6	
IC-IPMC	25	88.0	50.6	38.0	
Histology of invasive cancer in I-IPMC					
Tubular adenocarcinoma§	29	89.7	61.8	54.1	0.065
Pure mucinous carcinoma	12	100.0	100.0	57.1	
Tubular adenocarcinoma§	29	89.7	61.8	54.1	**0.010**
Nontubular adenocarcinoma	22	100.0	94.4	71.6	
Pure mucinous carcinoma	12	100.0	100.0	57.1	0.162
Nonpure mucinous carcinoma	39	92.3	68.6	62.9	
Past history of another cancer in other organs					0.316
+	10	90.0	72.0	54.0	
−	41	95.1	79.8	63.3	
TNM stage					
MI-IPMC	26	100.0	94.7	78.6	**0.040**
Stages IA, IB, and IIA	8	87.5	70.0	70.0	0.42
Stage IIB	13	84.6	56.4	0.0	0.82
Stages III and IV	4	100.0	25.0	25.0	

Statistically significant value is in bold characters.
*Diabetes mellitus exacerbation and jaundice included.
†Due to existence of neoplastic cells in pancreas margin in frozen section analysis.
‡Presence of invasive carcinoma cells in the stroma.
§Mixed tubular adenocarcinoma and mucinous carcinoma were included.
BD indicates branch duct; MPD, main pancreatic duct; Ph, pancreatic head; PV, portal vein.

carcinoma rather than IPMN itself that determines the prognosis.

In our series, none of the patients with MI-IPMCs showed LN metastasis, whereas the patients with IC-IPMCs had a high rate (68%) of LN metastasis. This finding implies that complete resection of a lesion without LN dissection may be sufficient for the treatment of MI-IPMC, whereas radical pancreatectomy with LN dissection is indicated for IC-IPMC. In this context, preoperative distinction between MI-IPMCs and IC-IPMCs is clinically very important.

TABLE 4. Multivariate Analysis of Effects of Clinicopathologic Factors on Postoperative Survival of I-IPMC

	Hazard Ratio	95% Confidence Interval	P*
IC-IPMC (vs. MI-IPMC)	7.1	1.9-26.5	<0.001
CA19-9 >300 (U/mL)	4.4	1.4-13.8	0.010

*P value was calculated by Cox hazards model (backward elimination method).

TABLE 5. Pancreatic Margin Status and the Recurrence of IPMNs After Surgery

	IPMA or Borderline IPMN (n = 38)	Noninvasive IPMC (n = 15)	MI-IPMC (n = 26)	IC-IPMC (n = 25)	Total (n = 104)	P
Additional pancreas resection*	3	0	5	9	17	0.007†
Final margin status						0.071
Negative	26	10	20 (2)	19 (11)	75	
IPMA	12	5	5	3 (1)‡	25	
Borderline IPMN	0	0	1	1	2	
Noninvasive IPMC	0	0	0	1	1	
Invasive cancer	0	0	0	1 (1)§	1	
Recurrence						
MI-IPMC (in the remnant pancreas)	0	0	1	0	1	
Invasive cancer (in the remnant pancreas)	0	0	1	0	1	
Local recurrence of invasive cancer	0	0	0	2	2	
Local LN	0	0	0	2	2	
Distant metastasis (lung or liver)	0	0	0	5	5	
Peritoneal dissemination	0	0	0	4	4	
Total	0	0	2	13	15	

*Due to the presence of neoplastic cells in the pancreatic surgical margin in the frozen section analysis.
†Comparison between noninvasive IPMN and I-IPMC.
‡Liver metastasis.
§Local recurrence, numbers in the parentheses denotes the number of patients who developed recurrence after the operation.

Another significant finding was a predominantly high recurrence rate among patients with IC-IPMC (52%), compared with 2.5% for patients with noninvasive IPMN or MI-IPMC. In the latter group, recurrence was observed in the remnant pancreas distant from the cut end, suggesting that IPMC occurred multifocally. Although this recurrence rate is not as high as that reported previously,[4] careful follow-up seems to be necessary after surgery, especially in patients with IC-IPMCs.

Our criteria are not contradictory to the previous studies, in which the postoperative outcome of I-IPMC with pure mucinous carcinoma (colloid carcinoma) was better than that of patients with I-IPMC with tubular adenocarcinoma in the invasive lesion.[1,24] Tubular adenocarcinoma shows active infiltrative growth similar to conventional pancreatic ductal adenocarcinoma, suggesting that it rapidly grows and progresses into advanced cancer. In fact, tubular adenocarcinoma occurred at a higher rate in IC-IPMC than in MI-IPMC, and was an unfavorable prognostic factor ($P = 0.010$; Table 3). It has been reported that mucinous carcinoma associated with IPMN or mucinous cystic tumor has a better outcome than conventional ductal carcinoma. According to Adsay's criteria (a carcinoma with more than 80% of mucinous carcinoma is defined as pure mucinous carcinoma),[1] 12 I-IPMCs were diagnosed as pure mucinous carcinoma associated with IPMC in our series, which contained 11 MI-IPMC (5 with infiltrative growth of pure mucinous carcinoma, 2 with predominantly mucous rupture with cellular component, and 4 with expansive growth) and 1 IC-IPMC. Among these 12 patients with pure mucinous carcinoma associated with IPMC, 1 patient with MI-IPMC with infiltrative growth and 1 patient with IC-IPMC had recurrence of the carcinoma. Although 12 patients had the recurrent cancers and 10 of them died among 29 patients of I-IPMCs with tubular adenocarcinoma (8 in MI-IPMC and 21 in IC-IPMC). Patients with pure mucinous carcinoma as histologic type of invasive cancer tended to have better prognosis than patients with tubular adenocarcinoma as invasive cancer ($P = 0.065$; Table 3). Our study also suggested that some mucinous carcinoma has aggressive behavior. The prognosis of mucinous carcinoma in the other organs such as colon, has been reported to be worse than the ordinary adenocarcinoma, especially worse for mucinous carcinoma with rich cellular component.[17,21] In ductal carcinoma of the pancreas, mixed mucinous carcinoma with other histologic types of carcinoma (usually tubular adenocarcinoma) shows bad prognosis comparable with the other types of conventional ductal adenocarcinoma.[7,14] In this situation, it is desired that a diagnostic criterion is established to distinguish aggressive and nonaggressive mucinous carcinoma correctly. In this study, addition to the classification of tubular adenocarcinoma of the I-IPMC into aggressive and nonaggressive state, we also classified mucinous carcinoma relevant to clinical behavior based on the invasiveness and cellularity. Compared with mucous rupture, more aggressive mucinous carcinoma shows massive invasion with much more cancer cells floating and proliferating in mucus lakes, and is often accompanied by partial invasion of tubular adenocarcinoma.

Lymphatic, venous, and intrapancreatic neural invasion were frequently observed in IC-IPMC (Table 2) and were significant prognostic factors in I-IPMC (Table 3). In this study, we tried to select early-stage I-IPMC with nonaggressive characters from I-IPMCs with such worse prognostic factors. We successfully selected it by categorizing the infiltrating depth of cancer cells, which included lymphatic, venous, and/or neural invasion. Indeed, all the patients with MI-IPMC having vessel or neural invasion within 5-mm length from IPMC duct

showed good postoperative outcome. In addition, lymphatic, venous, and intrapancreatic neural invasion were not significant variables for the prognosis in multivariate analysis (Table 4).

The present results suggest that IC-IPMC (not MI-IPMC) should be currently paid attention as I-IPMC with aggressive characteristics. In this situation, preoperative detection of IC-IPMC can be beneficial for selecting the most ideal operative procedure, especially on considering additional LN dissection. We are now investigating possible criteria for classifying these cancers preoperatively, and our findings suggest that it may be feasible to use radiologic data for this purpose. Multidetector row computed tomography was found to be useful to distinguish IC-IPMC from MI-IPMC and noninvasive IPMNs with more than 80% sensitivity and 100% specificity in the study using 123 patients with IPMNs (manuscript in preparation).

In future, we would like to test our criteria using another large series of samples or in a prospective study, to obtain more watertight pathologic criteria for classification of I-IPMC.

ACKNOWLEDGMENTS

The authors thank Drs Tsuyoshi Sano, Yoshihiro Sakamoto, Hidenori Ojima, and Minoru Esaki for useful discussions.

REFERENCES

1. Adsay NV, Merati K, Nassar H, et al. Pathogenesis of colloid (pure mucinous) carcinoma of exocrine organs. *Am J Surg Pathol*. 2003; 27:571–578.
2. Adsay NV, Merati K, Basturk O, et al. Pathologically and biologically distinct types of epithelium in intraductal papillary mucinous neoplasms. Delineation of an 'intestinal' pathway of carcinogenesis in the pancreas. *Am J Surg Pathol*. 2004;28:839–848.
3. Biankin AV, Kench JG, Dijkman FP, et al. Molecular pathogenesis of precursor lesions of pancreatic ductal adenocarcinoma. *Pathology*. 2003;35:14–24.
4. Chari ST, Yadav D, Smyrk TC, et al. Study of recurrence after surgical resection of intraductal papillary mucinous neoplasm of the pancreas. *Gastroenterology*. 2002;123:1500–1507.
5. Cho KR, Vogelstein B. Genetic alterations in the adenoma-carcinoma sequence. *Cancer*. 1992;70:1727–1731.
6. D'Angelica M, Brennan MF, Suriawinata AA, et al. Intraductal papillary mucinous neoplasms of the pancreas: an analysis of clinicopathologic features and outcome. *Ann Surg*. 2004;239:400–408.
7. Fukushima N, Mukai K, Kanai Y, et al. Intraductal papillary tumors and mucinous cystic tumors of the pancreas. *Hum Pathol*. 1997;28:1010–1017.
8. Furukawa T, Klöppel G, Volkan Adsay N, et al. Classification of types of intraductal papillary-mucinous neoplasm of the pancreas: a consensus study. *Virchows Arch*. 2005;447:794–799.
9. Hiraoka N, Onozato K, Kosuge T, et al. Prevalence of FOXP3$^+$ regulatory T cells increases during the progression of pancreatic ductal adenocarcinoma and its precursor lesions. *Clin Cancer Res*. 2006;12:5423–5434.
10. Hruban RH, Takaori K, Klimstra DS, et al. An illustrated consensus on the classification of pancreatic intraepithelial neoplasia and intraductal papillary mucinous neoplasms. *Am J Surg Pathol*. 2004;28:977–987.
11. International Union Against Cancer (UICC). *TNM Classification of Malignant Tumors*. 6th ed. New York, NY: Wiley-Liss; 2002.
12. Japan Pancreas Society. *Classification of Pancreatic Cancer*. 2nd ed. Tokyo, Japan: Kanehara; 2003.
13. Klöppel G, Solcia E, Longnecker DS, et al. *Histological Typing of Tumors of the Exocrine Pancreas, World Health Organization International Histological Classification of Tumors*. 2nd ed. Berlin, Germany: Springer; 1996.
14. Klöppel G, Hruban RH, Longnecker DS, et al. Ductal adenocarcinoma of the pancreas. In: Hamilton SR, Aaltonen LA, eds. *Pathology and Genetics. Tumours of the Digestive System. World Health Organization Classification of Tumours*. Lyon, France: IARC Press; 2000:221–230.
15. Longnecker DS, Adler G, Hruban RH, et al. Intraductal papillary-mucinous neoplasms of the pancreas. In: Hamilton SR, Aaltonen LA, eds. *Pathology and Genetics. Tumours of the Digestive System. World Health Organization Classification of Tumours*. Lyon, France: IARC Press; 2000:237–240.
16. Maire F, Hammel P, Terris B, et al. Prognosis of malignant intraductal papillary mucinous tumours of the pancreas after surgical resection. Comparison with pancreatic ductal adenocarcinoma. *Gut*. 2002;51:717–722.
17. Minsky BD, Mies C, Rich TA, et al. Colloid carcinoma of the colon and rectum. *Cancer*. 1987;60:3103–3112.
18. Mizuta Y, Akazawa Y, Shiozawa K, et al. Pseudomyxoma peritonei accompanied by intraductal papillary mucinous neoplasm of the pancreas. *Pancreatology*. 2005;5:470–474.
19. Nakagohri T, Asano T, Kenmochi T, et al. Long-term surgical outcome of noninvasive and minimally invasive intraductal papillary mucinous adenocarcinoma of the pancreas. *World J Surg*. 2002;26:1166–1169.
20. Raimondo M, Tachibana I, Urrutia R, et al. Invasive cancer and survival of intraductal papillary mucinous tumors of the pancreas. *Am J Gastroenterol*. 2002;97:2553–2558.
21. Ronnett BM, Zahn CM, Kurman RJ, et al. A Clinicopathologic analysis of 109 cases with emphasis on distinguishing pathologic features, site of origin, prognosis, and relationship to "pseudomyxoma peritonei". *Am J Surg Pathol*. 1995;19:1390–1408.
22. Salvia R, Fernandez-del Castillo C, Bassi C, et al. Main-duct intraductal papillary mucinous neoplasms of the pancreas: clinical predictors of malignancy and long-term survival following resection. *Ann Surg*. 2004;239:677–678.
23. Shimada K, Sakamoto Y, Sano T, et al. Invasive carcinoma originating in an intraductal papillary mucinous neoplasm of the pancreas: a clinicopathologic comparison with a common type of invasive ductal carcinoma. *Pancreas*. 2006;32:281–287.
24. Sohn TA, Yeo CJ, Cameron JL, et al. Intraductal papillary mucinous neoplasms of the pancreas: an updated experience. *Ann Surg*. 2004;239:788–789.
25. Suzuki Y, Atomi Y, Sugiyama M. Cystic neoplasm of the pancreas: a Japanese multi-institutional study of intraductal papillary mucinous tumor and mucinous cystic tumor. *Pancreas*. 2004;28:241–246.
26. Wells M, Östör AG, Crum CP, et al. Epithelial tumours. In: Tavassoli FA, Devilee P, eds. *Pathology and Genetics of Tumours of the Breast and Female Genital Organs. World Health Organization Classification of Tumours*. Lyon, France: IARC Press; 2003: 262–269.
27. Yamao K, Ohashi K, Nakamura T, et al. The prognosis of intraductal papillary mucinous tumors of the pancreas. *Hepatogastroenterology*. 2000;47:1129–1134.

Frequent Inactivation of a Putative Tumor Suppressor, Angiopoietin-Like Protein 2, in Ovarian Cancer

Ryoko Kikuchi,[1,6,7,8] Hitoshi Tsuda,[4,6,7] Ken-ichi Kozaki,[1,2,6] Yae Kanai,[4] Takahiro Kasamatsu,[5] Kazuo Sengoku,[5] Setsuo Hirohashi,[4] Johji Inazawa,[1,2,3,6] and Issei Imoto[1,2,6]

[1]Department of Molecular Cytogenetics, Medical Research Institute and School of Biomedical Science, [2]Hard Tissue Genome Research Center, and [3]21st Century Center of Excellence Program for Molecular Destruction and Reconstitution of Tooth and Bone, Tokyo Medical and Dental University, Tokyo, Japan; [4]Pathology Division, National Cancer Center Research Institute and [5]Division of Gynecology, National Cancer Center Hospital, Tokyo, Japan; [6]Core Research for Evolutional Science and Technology, Japan Science and Technology Corporation, Kawagoe, Japan; [7]Department of Basic Pathology, National Defense Medical College, Tokorozawa, Japan; and [8]Department of Obstetrics and Gynecology, Asahikawa Medical College, Asahikawa, Japan

Abstract

Angiopoietin-like protein 2 (ANGPTL2) is a secreted protein belonging to the angiopoietin family, the members of which are implicated in various biological processes, although its receptor remains unknown. We identified a homozygous loss of *ANGPTL2* (9q33.3) in the course of screening a panel of ovarian cancer (OC) cell lines for genomic copy-number aberrations using in-house array-based comparative genomic hybridization. *ANGPTL2* mRNA expression was observed in normal ovarian tissue and immortalized normal ovarian epithelial cells, but was reduced in some OC lines without its homozygous deletion (18 of 23 lines) and restored after treatment with 5-aza 2′-deoxycytidine. The methylation status of sequences around the *ANGPTL2* CpG-island with clear promoter activity inversely correlated with expression. *ANGPTL2* methylation was frequently observed in primary OC tissues as well. In an immunohistochemical analysis of primary OCs, ANGPTL2 expression was frequently reduced (51 of 100 cases), and inversely correlated with methylation status. Patients with OC showing reduced ANGPTL2 immunoreactivity had significantly worse survival in the earlier stages (stages I and II), but better survival in advanced stages (stages III and IV). The restoration of ANGPTL2 expression or treatment with conditioned medium containing ANGPTL2 inhibited the growth of OC cells originally lacking the expression of this gene, whereas the knockdown of endogenous ANGPTL2 accelerated the growth of OC cells with the expression of ANGPTL2. These results suggest that, at least partly, epigenetic silencing by hypermethylation of the *ANGPTL2* promoter leads to a loss of ANGPTL2 function, which may be a factor in the carcinogenesis of OC in a stage-dependent manner. [Cancer Res 2008;68(13):5067–75]

Introduction

Epithelial ovarian cancer (OC) is the most common and lethal gynecologic malignancy and is one of the leading causes of cancer mortality in women because the disease usually presents at an advanced stage, as there are no overt symptoms at early stages (1, 2). Despite the use of primary surgical cytoreduction and systemic administration of paclitaxel-containing and platinum-containing chemotherapy regimens, minimal improvements have been made in overall survival over the past three decades. Therefore, a critical need exists for the identification of molecular markers and targets for diagnosis as well as therapy, which will come from a better understanding of the molecular mechanisms responsible for the tumorigenesis of this disease (3).

Sporadic OCs often show complex, aneuploid karyotypes, with a myriad of nonrandom structural chromosomal abnormalities (4), which may activate oncogenes or inactivate tumor suppressor genes (TSG) during the transformation process. To identify novel candidates for TSGs, homozygously deleted regions within the cancer cell genome are likely to serve as a good landmark (5–9), although biallelic loss is a rare event, and other factors, such as point mutations and epigenetic abnormalities (10), may predominantly contribute to functional inactivation. Therefore, high-resolution mapping of homozygous deletions within the entire genome of cancer cells would be of considerable help in the rapid identification of TSGs. Recently, we have applied an in-house bacterial artificial chromosome (BAC)–based array containing 800 BAC clones (MCG Cancer Array-800; ref. 5) to an array-based comparative genomic hybridization (array-CGH) analysis of OC cell lines, and identified connective tissue growth factor (*CTGF/CCN2*) as a putative ovarian TSG mainly inactivated by DNA methylation from homozygous loss at 6q23 (11). Because (*a*) there is no doubt that carcinoma is the result of the accumulation of multiple somatic genetic and/or epigenetic alterations resulting in either the activation of oncogenes or the inactivation of TSGs and (*b*) homozygous loss is usually small, more TSGs involved in the ovarian carcinogenesis will be identified through the genome-wide search for copy-number changes using arrays with a higher resolution, as shown in our previous studies in various other cancers (12–14).

In the report presented here, we have employed an in-house BAC array with an average spacing of 0.7 Mb (MCG Whole Genome Array-4500), which has ~5.6-fold higher resolution than MCG Cancer Array-800 (5), to a panel of OC cell lines for genomewide copy-number analysis. During the course of these experiments, we identified a novel homozygous loss at 9q33.3 containing angiopoietin-like protein 2 (*ANGPTL2*), the expression of which was absent in some OC cell lines without homozygous loss, although it was present in the normal ovary. To clarify the mechanism and the effect on ovarian carcinogenesis of down-regulated ANGPTL2 expression, we further determined the expression and methylation status of *ANGPTL2* and their clinicopathologic and functional significance in OC.

Note: Supplementary data for this article are available at Cancer Research Online (http://cancerres.aacrjournals.org/).

Requests for reprints: Johji Inazawa, Department of Molecular Cytogenetics, Medical Research Institute, Tokyo Medical and Dental University, 1-5-45 Yushima, Bunkyo-ku, Tokyo 113-8510, Japan. Phone: 81-3-5803-5820; Fax: 81-3-5803-0244; E-mail: johinaz.cgen@mri.tmd.ac.jp.

doi:10.1158/0008-5472.CAN-08-0062

Materials and Methods

Cell lines and primary tumors. Twenty-four OC cell lines whose derivation and sources have been previously reported (11) were used. The immortalized normal ovarian epithelial cell line OSE-2a (15), kindly provided by Dr. Hidetaka Katabuchi (Kumamoto University School of Medicine, Kumamoto, Japan), was used as a normal control. All cell lines were maintained in appropriate medium supplemented with 10% fetal bovine serum, 100 units/mL of penicillin, and 100 μg/mL of streptomycin. To prepare a conditioned medium, SAS, an oral squamous cell carcinoma cell line that grows in serum-free DMEM/F12 (1:1), was used.

Primary OC tumor samples were obtained during surgery from 100 patients being treated at the National Cancer Center Hospital in Tokyo, with written consent from each patient in the formal style and after approval by the local ethics committee, and were embedded in paraffin for immunohistochemistry. Samples from 45 of these patients were immediately frozen in liquid nitrogen and stored at −80°C until required. DNA of a quality good enough for a methylation analysis was obtained from each of the 45 samples, whereas RNA of a quality good enough for an expression analysis was obtained from only 4 samples. None of the patients had received preoperative radiation or immunotherapy. All patients underwent complete surgical staging, including i.p. cytology, bilateral salpingo-oophorectomy, hysterectomy, omentectomy, and pelvic/para-aortic lymphadenectomy. Aggressive cytoreductive surgery was conducted in patients with advanced disease. Surgical staging was based on the International Federation of Gynecology and Obstetrics staging system: stage I, 53 patients; stage II, 11 patients; stage III, 28 patients; and stage IV, 8 patients.

Array-CGH. Array-CGH using a MCG Whole Genome Array-4500 (5) was carried out as described elsewhere (13). Images acquired by a GenePix 4000B (Axon Instruments) were analyzed with GenePix Pro 6.0 software (Axon Instruments). After normalization, average ratios that deviated significantly (>2 SD) from 0 ($\log_2$ ratio, <−0.4 and >0.4) were considered abnormal.

PCR. Homozygous deletions were detected by genomic PCR (11, 13). For expression analyses, single-stranded cDNA generated from total RNA was amplified with primers specific for each gene (16). The glyceraldehyde-3-phosphate dehydrogenase (*GAPDH*) gene was amplified at the same time to allow the estimation of the efficiency of cDNA synthesis. For conventional reverse transcription-PCR (RT-PCR), PCR products were electrophoresed, whereas quantitative real-time RT-PCR was done with an ABI Prism 7900 Sequence Detection System (Applied Biosystems). Each assay was conducted in triplicate. All primer sequences are listed in Supplementary Table S1.

Drug treatment. OC cells were cultured with various concentrations of 5-aza 2′-deoxycytidine (5-aza-dCyd) for 5 days and/or 100 ng/mL of trichostatin A (TSA) for the last 12 h.

Methylation analysis. Genomic DNA was treated with sodium bisulfite, and subjected to PCR using primers to amplify regions of interest (Supplementary Table S1). For the combined bisulfite restriction analysis (COBRA), a semiquantitative bisulfite-PCR analysis (17), PCR products were digested with *Bst*UI and electrophoresed. For bisulfite sequencing, PCR products were subcloned and then sequenced. For the methylation-specific PCR (MSP) analysis, sodium bisulfite–treated DNA was subjected to PCR using primer sets specific to the methylated and unmethylated forms of DNA sequences, and PCR products were visualized on 3% agarose gels. DNA from cell lines recognized as unmethylated by bisulfite sequencing was used as negative controls for methylated alleles, whereas DNA from lines recognized as methylated or CpGenome Universal Methylated DNA (Chemicon International) was used as positive controls.

Promoter reporter assay. DNA fragments around the *ANGPTL2* CpG-island were obtained by PCR and ligated into the reporter vector pGL3-Basic (Promega). The reporter assay was performed as described elsewhere (11) using each construct or an empty vector with an internal control pRL-hTK (Promega).

Western blotting. For Western blotting, cell lysates were analyzed as described elsewhere (11). Anti-ANGPTL2, anti-Myc-Tag, and anti-β-actin antibodies were purchased from R&D Systems, Cell Signaling Technology, and Sigma, respectively.

Immunohistochemistry. Indirect immunohistochemistry was performed with formalin-fixed, paraffin-embedded tissue sections as described elsewhere (11). After blocking in 2% normal swine serum, the slides were incubated with an anti-ANGPTL2 antibody (1:500 dilution; R&D Systems) and then reacted with a Histofine simple stain, MAX PO(G) (Nichirei). Antigen-antibody reactions were visualized with 0.2% diaminobenzidine tetrahydrochloride and hydrogen peroxide. The slides were counterstained with Mayer's hematoxylin.

Formalin-fixed HT cells expressing *ANGPTL2* mRNA, >50% of which showed cytoplasmic staining of ANGPTL2 protein, and KF28 cells lacking *ANGPTL2* mRNA expression, none of which showed staining of ANGPTL2 protein, were used as positive and negative controls, respectively. The specificity of the antibody was verified by Western blotting. The percentage of the total cell population that expressed ANGPTL2 was evaluated for each case at ×200 magnification. Expression of ANGPTL2 was graded as either positive (>10% of tumor cell cytoplasm showing immunopositivity, 49 tumors) or negative (<10% of tumor cell cytoplasm showing immunopositivity or no staining, 51 tumors) according to the results in our preliminary analyses (Supplementary Fig. S1).

Growth assay. For colony formation assays (11), a plasmid expressing COOH-terminal Myc-tagged and His-tagged ANGPTL2 (pcDNA3.1-ANGPTL2-Myc-His) was obtained by cloning the PCR product of the full coding sequence of *ANGPTL2* in-frame along with the Myc and 6xHis epitopes into pcDNA3.1 (Invitrogen). pcDNA3.1-ANGPTL2-Myc-His, or the empty vector (pcDNA3.1-mock), was transfected into cells. Cells were stained with crystal violet after 2 weeks of incubation in six-well plates with appropriate concentrations of G418.

To assess the effect of ANGPTL2 on the growth of OC cell lines, cells were treated with the conditioned medium containing ANGPTL2 (18). pcDNA3.1-ANGPTL2-Myc-His or pcDNA3.1-mock was introduced into SAS cells lacking the expression of ANGPTL2. Cells were washed thrice with serum-free medium 24 h after transfection, and then cultured for 4 days. Media were changed everyday. The obtained conditioned media were centrifuged, and supernatants were pooled, concentrated (1:100) with the Amicon Ultra-15 YM-50 (Millipore), sterilized with a Costar Spin-X Centrifuge Tube Filter (Corning), and stored at −80°C prior to use. OC cell lines lacking the expression of *ANGPTL2* were treated with medium containing 0.2% fetal bovine serum and 1% concentrated conditioned medium. The number of viable cells after treatment were assessed by a colorimetric water-soluble tetrazolium salt (WST) assay (11). The cell cycle in ANGPTL2-treated cells was analyzed using fluorescence-activated cell sorting (FACS) as described elsewhere (11).

ANGPTL2-specific small interfering RNA (siRNA; *ANGPTL2*-siRNA) was purchased from Dharmacon. A control siRNA for the luciferase gene (CGUACGCGGAAUACUUCGA, *Luc*-siRNA) was synthesized by Sigma. Each siRNA (50 nmol/L) was introduced into OC cells using LipofectAMINE RNAiMAX (Invitrogen). The number of viable cells 24 to 96 h after transfection was assessed by WST assay.

Statistical analysis. Differences between subgroups were tested with the Mann-Whitney *U* test. Correlations between *ANGPTL2* methylation or expression in primary OCs and the clinicopathologic variables pertaining to the corresponding patients were analyzed for statistical significance with χ^2 or Fisher's exact test. For analysis survival, Kaplan-Meier survival curves were constructed for groups based on univariate predictors, and differences between the groups were tested with the log-rank test. Differences were assessed with a two-sided test and considered significant at the $P < 0.05$ level.

Results

Array-CGH analysis of OC cell lines. In the array-CGH analysis using an MCG Whole Genome Array-4500, frequently detected copy-number gains and losses within the entire genome of 24 OC cell lines (data not shown) were the same as those in our previous

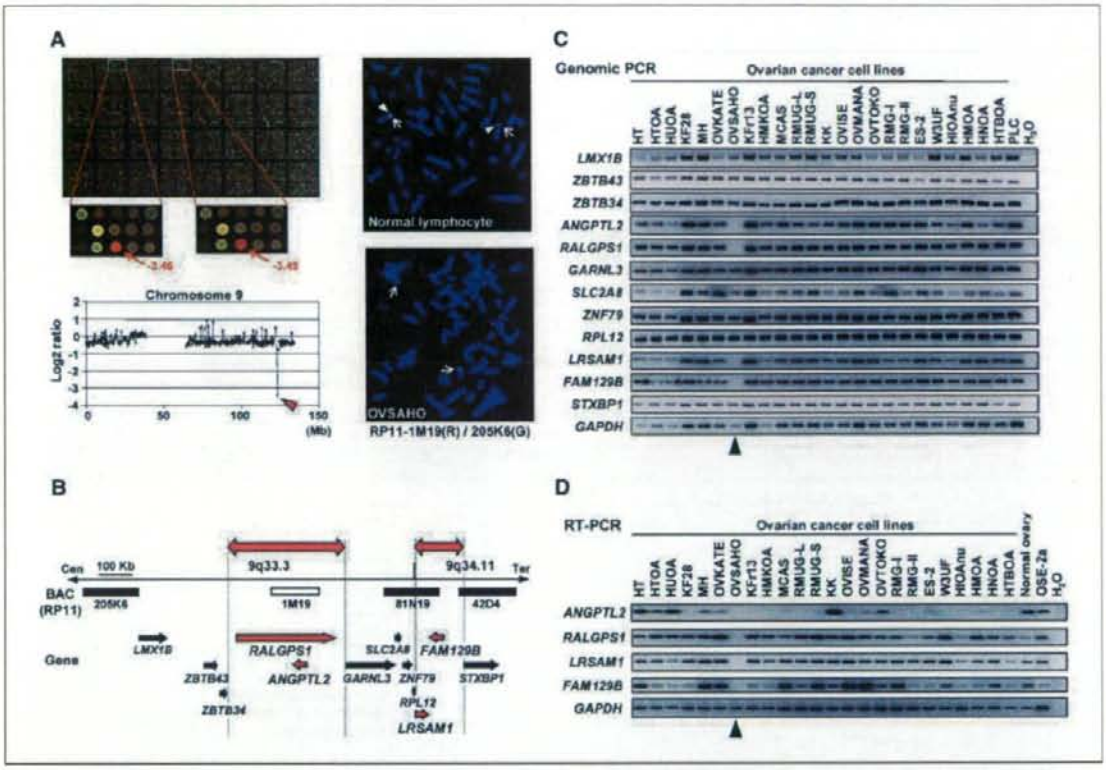

Figure 1. *A*, identification of the 9q33.3 homozygous deletion in the OC cell line. *Top left*, duplicate array-CGH image (MCG Whole Genome Array-4500) of the OVSAHO cell line. A homozygous deletion (copy-number ratio as $\log_2$ ratio) of the BAC clone at 9q33.3 was detected as a clear red signal (*red arrows*). *Bottom left*, representative copy-number profiles of chromosome 9 in OVSAHO cells. *Red arrowhead*, candidate spots (RP11-1M19) showing patterns of homozygous deletion ($\log_2$ ratio <−2). *Right*, FISH image from probe RP11-1M19 (*red signals, arrowheads*) and with RP11-205K6 as a control (*green signals, arrows*) hybridized to metaphase chromosomes from the control normal peripheral lymphocyte (*top*) and OVSAHO cell line (*bottom*). The absence of red signals indicates homozygous loss of sequences within RP11-1M19 in the OVSAHO cell line. *B*, map of 9q33.3-q34.11 covering the region homozygously deleted in the OVSAHO cell line. BAC (RP11-1M19) was homozygously deleted in the array-CGH analysis (*vertical white bar*). The homozygously deleted region in OVSAHO cells, as determined by genomic PCR analysis (*vertical red closed arrow*). Ten genes located within this region (*red arrows*, homozygously deleted genes; *black arrows*, retained genes) showing the positions and directions of transcription. *C*, genomic PCR analyses of genes located around the 9q33.3-9q34.11 homozygously deleted region in OC cell lines. Homozygous deletions of *ANGPTL2*, *RALGPS1*, *LRSAM1*, and *FAM129B* but not *LMX1B*, *ZBTB43*, *ZBTB34*, *GARNL3*, *SLC2A8*, *ZNF79*, *RPL12*, and *STXBP1* were detected in one OC cell line (*OVSAHO*, *arrowhead*) by genomic PCR. *D*, mRNA expression of *ANGPTL2*, *RALGPS1*, *LRSAM1*, and *FAM129B* in OC cell lines and the normal ovary and normal ovarian epithelial cell–derived cell line OSE-2a, detected by RT-PCR. *Arrowhead*, a cell line with the homozygous deletion indicated in the genomic PCR analysis. Expression of *RALGPS1*, *LRSAM1*, and *FAM129B* mRNAs was observed to some degree in most OC cell lines, whereas *ANGPTL2* showed frequent silencing. Notably, 18 of the 23 cell lines (78%) without a homozygous deletion of *ANGPTL2* showed decreased expression.

study (11). Compared with the MCG Cancer Array-800, we identified more homozygous deletions ($\log_2$ ratio <−2) and high-level amplifications ($\log_2$ ratio > 2), which are likely to be landmarks of TSGs and oncogenes, respectively, using the MCG Whole Genome Array-4500: homozygous deletions at 4q, 6q, 8q, 9p, and 9q (Supplementary Table S2), and amplifications at 2q, 11q, and 19q (Supplementary Table S3). All these alterations were confirmed by fluorescence *in situ* hybridization (Fig. 1*A*; data not shown). Among them, the homozygous loss at 9q33.3 observed in OVSAHO cells had never been previously documented in OC, prompting us to examine whether genes located within this region are involved in the pathogenesis of OC.

Identification of target genes involved in homozygous deletion at 9q33.3. To define the extent of the homozygous loss at 9q33.3 in OVSAHO cells and to identify other OC lines harboring a cryptic homozygous loss in this region, we performed genomic PCR with 12 genes (*LMX1B, ZBTB43, ZBTB34, RALGPS1, ANGPTL2, GARNL3, SLC2A8, ZNF79, RPL12, LRSAM1, FAM129B*, and *STXBP1*; Fig. 1*B*) located around RP11-1M19 according to information archived by genome databases.[9,10] We detected a complete loss of *ANGPTL2, RALGPS1, LRSAM1*, and *FAM129B* only in OVSAHO cells, whereas *LMX1B, ZBTB43, ZBTB34, GARNL3, SLC2A8, ZNF79, RPL12*, and *STXBP1* were retained in this cell line (Fig. 1*C*), indicating that the homozygous deletion has a structurally complicated pattern, and its total size is ~0.55 Mb at maximum.

[9] http://www.ncbi.nlm.nih.gov/
[10] http://genome.ucsc.edu/

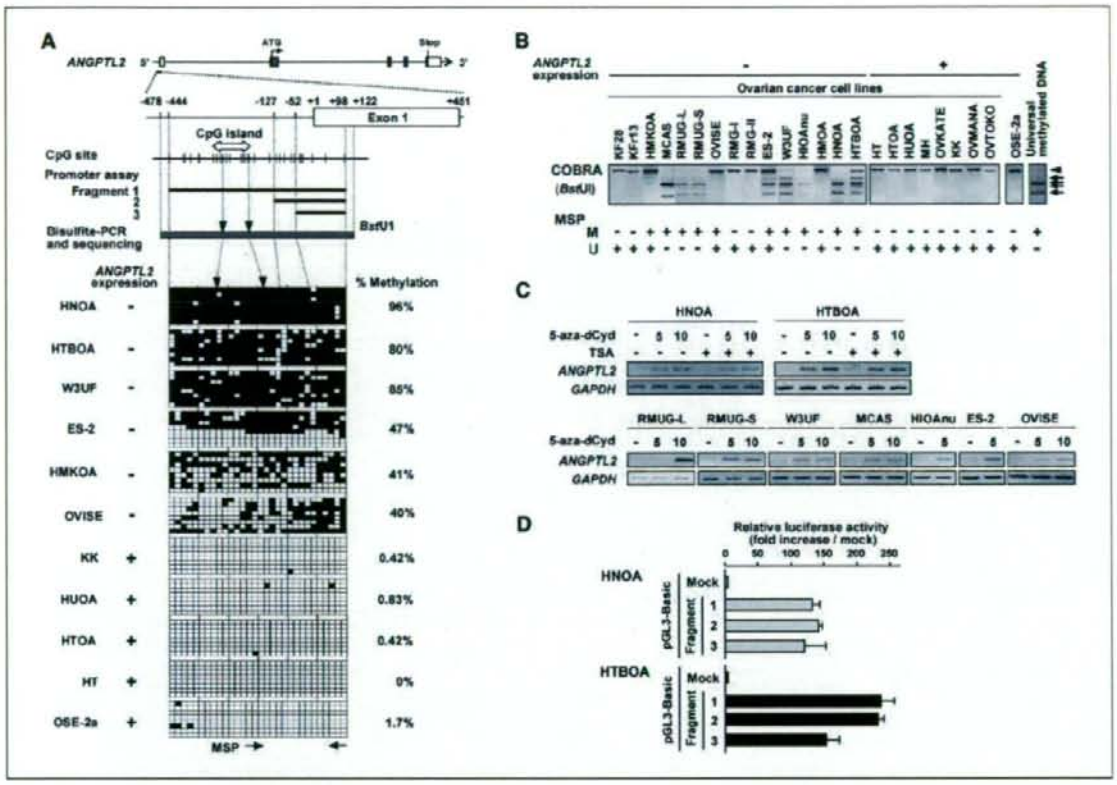

Figure 2. Methylation status of the *ANGPTL2* CpG-rich region in OC cell lines. *A*, schematic map of the CpG-rich region containing the CpG-island (*closed white arrow*) around exon 1 of *ANGPTL2* and representative results of bisulfite sequencing. CpG sites (*vertical ticks*), exons (*open box*), and the transcription-start site (*marked at +1*) on the expanded axis. *Thick black lines*, the fragments examined in a promoter assay; *horizontal gray bar*, the regions examined in the COBRA and bisulfite sequencing; *black downward arrowheads*, restriction sites for *Bst*UI in COBRA. Representative results of bisulfite sequencing of the *ANGPTL2* CpG-rich region examined in *ANGPTL2*-expressing OC cell lines (+) and nonexpressing OC cell lines (−). Each square indicates a CpG site: *open squares*, unmethylated; *solid squares*, methylated. *Arrows*, PCR primers for MSP. *B*, representative results of the COBRA of the *ANGPTL2* CpG-island in OC cell lines after restriction with *Bst*UI. *Arrows*, fragments specifically restricted at sites recognized as methylated CpGs; *arrowheads*, undigested fragments indicating unmethylated CpGs. Results of the MSP analysis are also shown. *M*, methylated allele; *U*, unmethylated allele. Representative images of MSP are shown in Supplementary Fig. S2. CpGenome Universal Methylated DNA (Chemicon International) was used as positive controls for methylation analyses. *C*, representative results of RT-PCR to reveal restored *ANGPTL2* expression after demethylation in cell lines lacking its expression. *Top*, restored *ANGPTL2* expression in HNOA and HTBOA cell lines after treatment with 5-aza-dCyd (5 or 10 μmol/L) for 5 d with or without TSA (100 ng/mL) for the last 12 h. Notably, almost no effect of TSA treatment on *ANGPTL2* expression was observed in cells either with or without 5-aza-dCyd treatment. *Bottom*, restored *ANGPTL2* expression in RMUG-L, RMUG-S, W3UF, MCAS, HIOAnu, ES-2, and OVISE cell lines after treatment with 5-aza-dCyd, which showed reduced expression of *ANGPTL2* mRNA (Fig. 1*D*) and a methylated pattern (Fig. 1*B*). *D*, promoter activity of the *ANGPTL2* CpG-rich region around the CpG-island. pGL3 basic empty vectors (mock) and constructs containing one of three different sequences around the highly methylated region of *ANGPTL2* (fragments 1–3; 542, 225, and 150 bp in size, respectively, in *A*) were transfected into HNOA and HTBOA cells. Luciferase activity was normalized vs. an internal control. *Columns*, means for three separate experiments, each performed in triplicate; *bars*, SD.

Loss of *ANGPTL2* expression in OC cell lines. Next, we determined the mRNA expression levels of *ANGPTL2*, *RALGPS1*, *LRSAM1*, and *FAM129B* by RT-PCR in all 24 OC lines, normal ovary, and the OSE-2a cell line. *RALGPS1*, *LRSAM1*, and *FAM129B* were expressed in most of the OC lines at levels similar to or higher than those in normal ovary and/or the OSE-2a cell line (Fig. 1*D*). On the other hand, *ANGPTL2* mRNA was frequently silenced in OC lines without the homozygous deletion (18 of 23, 78%; Fig. 1*D*), but was expressed in normal ovary and OSE-2a cells, suggesting that this gene is likely to be the most probable target for inactivation through mechanisms other than genomic deletion in OC cells. Because aberrant methylation within the CpG-island around the transcription start site (TSS) of genes is known to be one of the key mechanisms by which TSGs can be silenced (9), and the CpGPLOT program[11] identified the CpG-island around the TSS of *ANGPTL2*, we focused on *ANGPTL2* for further DNA methylation analyses. None of the two lines that had shown a hemizygous loss around *ANGPTL2* in array-CGH exhibited a decreased expression of this gene (data not shown).

Methylation of the *ANGPTL2* CpG-island in OC cell lines. To show the potential role of methylation within the CpG-island in the silencing of *ANGPTL2*, we first assessed the methylation status of each CpG site around the *ANGPTL2* CpG-island (Fig. 2*A*) in OC lines with or without *ANGPTL2* expression and the OSE-2a cells, by

[11] http://www.ebi.ac.uk/emboss/cpgplot/

means of bisulfite sequencing. CpG sites around the *ANGPTL2* CpG-island tended to be extensively (HNOA, HTBOA, and W3UF) or partially (ES-2, OVISE, and HMKOA) methylated in the non-expressing cell lines, whereas *ANGPTL2*-expressing OC lines (KK, HUOA, HTOA, and HT) and OSE-2a cells were almost unmethylated (Fig. 2*B*). We then compared the methylation and expression status of *ANGPTL2* in a larger number of OC lines by COBRA covering the region around the CpG-island (Fig. 2*A*) and MSP designed to target the region around TSS (Fig. 2*A*), because two *Bst*UI restriction sites for COBRA may fail to detect DNA methylation around TSS. Consistent with the results of bisulfite sequencing, no methylated allele was detected among any of the OC cell lines with *ANGPTL2* expression and OSE-2a cells with either method (Fig. 2*B*; Supplementary Fig. S2). On the other hand, a methylated allele was detected in 10 of 15 OC cell lines lacking *ANGPTL2* expression by either method, although some of these cell lines retained an unmethylated allele. Five of the 15 OC cell lines (KF28, KFr13, RMG-I, RMG-II, and HMOA) lacking *ANGPTL2* expression were found to have only an unmethylated allele by either method, suggesting that mechanisms other than DNA methylation, including epigenetic silencing of transcription factors regulating *ANGPTL2* transcription, or upstream components of the signaling pathway activating *ANGPTL2* expression, also contribute to the silencing of *ANGPTL2* directly or indirectly.

To investigate whether DNA demethylation could restore the expression of *ANGPTL2* mRNA, we treated OC cells lacking *ANGPTL2* expression with 5-aza-dCyd. The induction of *ANGPTL2* mRNA expression occurred after treatment with 5 or 10 μmol/L of

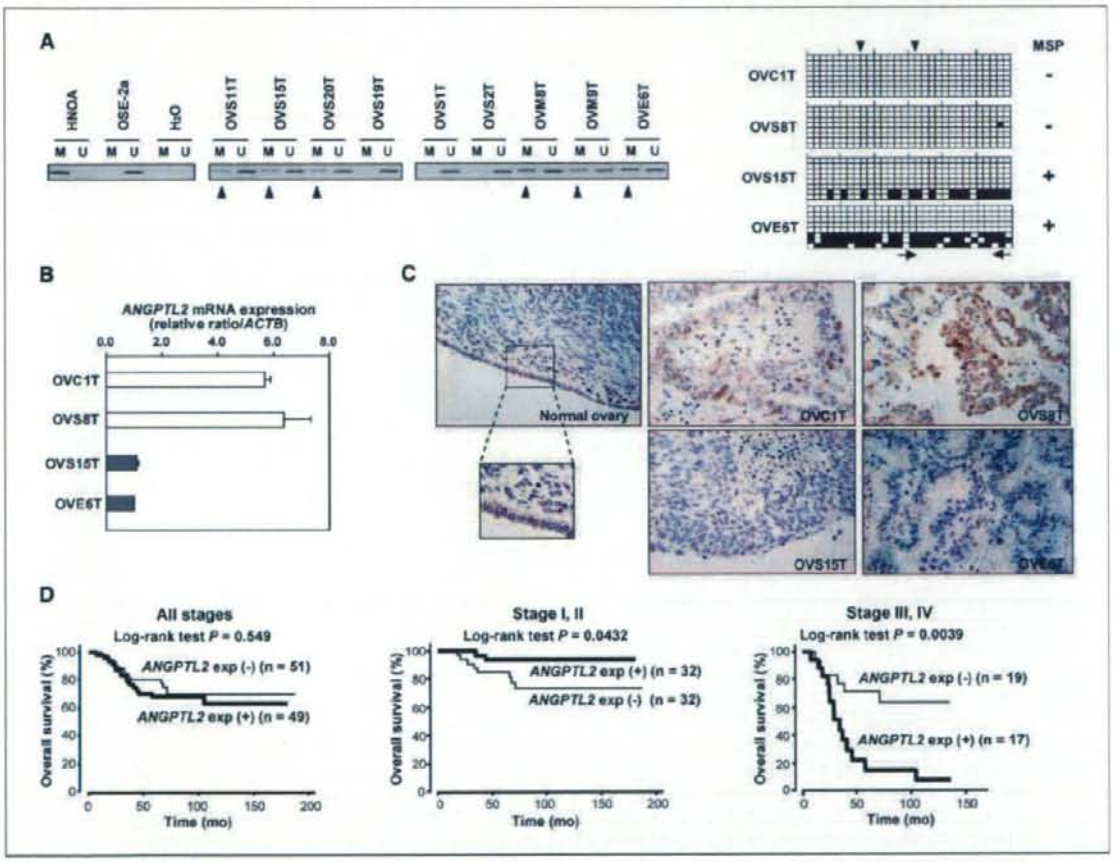

Figure 3. Methylation and expression status of *ANGPTL2* in primary tumors of OC. *A*, representative results of a MSP analysis (*left*) and bisulfite sequencing (*right*) of the *ANGPTL2* promoter region in primary OC tissues. *Left*, in the MSP analysis, parallel amplification reactions were performed using primers specific for unmethylated (*U*) or methylated (*M*) DNA. *Right*, methylation status of *ANGPTL2* determined by bisulfite sequencing in tumor samples. See legend of Fig. 2*A* for interpretation. *B*, representative results indicating an inverse correlation between methylation status of *ANGPTL2* determined by MSP and mRNA expression status determined by quantitative real-time RT-PCR in four primary tumors. *C*, representative results of immunohistochemical staining of ANGPTL2 protein in normal human ovarian epithelial cells and primary OC tumors. ANGPTL2 expression is shown in normal ovarian epithelial cells (*top left*). In primary OC, strong (*OVC1T* and *OVS8T*) or very weak (*OVS15T* and *OVE8T*) expression of ANGPTL2 was observed (original magnification, ×200). *D*, Kaplan-Meier curves for overall survival rates of patients at all stages (*left*), stage I and II (*middle*), and stage III and IV OC (*right*). In overall survival, no significant difference was observed between the patients with positive ANGPTL2 expression and those with negative ANGPTL2 expression in all stages ($P = 0.600$). In stage I and II disease, however, negative ANGPTL2 immunoreactivity in tumor cells was significantly associated with a worse overall survival ($P = 0.0432$), whereas positive ANGPTL2 immunoreactivity was significantly associated with a worse overall survival in stage III and IV disease ($P = 0.0039$).

Table 1. Correlation between clinical background and expression of ANGPTL2 protein

	Total (*n*)	Expression of ANGPTL2, *n* (%)*	*P*†
Total	100	49 (49)	
Age (y)			
<60	69	34 (49)	0.935
≥60	31	15 (48)	
FIGO stage			
I, II	64	32 (50)	0.790
III, IV	36	17 (47)	
Histologic type			
Serous	41	16 (39)	0.168
Mucinous	14	11 (79)	
Clear cell	34	17 (50)	
Endometrioid	11	5 (45)	
Optimal surgery‡			
Optimal (<2 cm)	82	38 (46)	0.217
Suboptimal (≥2 cm)	13	9 (69)	
Peritoneal cytology‡			
Positive	46	23 (50)	0.765
Negative	49	23 (47)	
Methylation§			
Positive	11	2 (18)	**0.0402**
Negative	34	19 (56)	

NOTE: Statistically significant values are in boldface type.

Abbreviation: FIGO, International Federation of Gynecology and Obstetrics.

*ANGPTL2 protein expression was evaluated by immunohistochemical analysis as described in Materials and Methods.

† *P* values are from χ^2 or Fisher's exact test and were statistically significant when <0.05 (two-sided).

‡ No information was available in five cases.

§ No high-quality DNA for methylation analysis was available in 55 cases.

5-aza-dCyd in HNOA and HTBOA cell lines (Fig. 2*C*). In addition, treatment with TSA had no effect on the *ANGPTL2* mRNA expression with or without 5-aza-dCyd in those cell lines, suggesting that DNA methylation is of primary importance for epigenetic silencing in OC cell lines. Restoration of *ANGPTL2* expression by 5-aza-dCyd was also observed in other cell lines, such as RMUG-L, RMUG-S, W3UF, MCAS, HIOAnu, ES-2, and OVISE, lacking expression and showing methylation of *ANGPTL2* in the COBRA and/or MSP analyses (Fig. 2*C*). Among *ANGPTL2* nonexpressing cell lines showing no methylation pattern in both COBRA and MSP analyses, almost no restoration of *ANGPTL2* expression was observed in RMG-I, RMG-II, and KFr13 cell lines, whereas a little restoration was observed in HMOA and KF28 cell lines by 5-aza-dCyd alone (Supplementary Fig. S3). TSA alone did not affect the expression of *ANGPTL2* in those lines, but induced expression in combination with 5-aza-dCyd in some cell lines (Supplementary Fig. S3).

Promoter activity of the sequence around the *ANGPTL2* CpG-island. Because the sequence around the *ANGPTL2* CpG-island seems to be a target for methylation-mediated gene silencing, we tested three fragments designed according to the results of bisulfite sequencing for promoter activity (fragments 1–3 in Fig. 2*A*). All three fragments showed a remarkable increase in transcriptional activity in HNOA and HTBOA lines (Fig. 2*D*), suggesting that the region around the *ANGPTL2* CpG-island, especially the sequence around TSS, contains critical sequences for basal gene expression and may be a target for methylation.

Analysis of *ANGPTL2* methylation and expression in primary OC tumors. To determine if the aberrant methylation of *ANGPTL2* also takes place in primary tumors of OC, we did MSP analysis with primer sets targeting the sequence around the most frequently methylated sites (Fig. 2*A*) in 45 primary cases. Consistent with the results of bisulfite sequencing and COBRA (Fig. 2*A* and *B*), a representative cell line lacking *ANGPTL2* expression (HNOA) was methylated, whereas the *ANGPTL2*-expressing cell line (OSE-2a) was unmethylated (Fig. 3*A*). We detected *ANGPTL2* hypermethylation in 11 of the 45 primary OCs (24%; Supplementary Table S4; Fig. 3*A*; data not shown). To quantitatively confirm the results of MSP analysis, we performed bisulfite sequencing in some representative cases. Aberrant methylation in a pattern similar to that observed in OC lines lacking *ANGPTL2* expression was observed in OC tissues, which showed a methylation pattern in the MSP, whereas tumors with an unmethylated pattern in the MSP showed hypomethylation in bisulfite sequencing (Fig. 3*A*; data not shown).

In four cases of OC in which tumor samples were available for triple analyses, i.e., a methylation analysis, real-time RT-PCR, and immunohistochemistry, we compared the expression status of *ANGPTL2* with its methylation status (Fig. 3*A–C*). Methylation-positive tumors tended to express fewer *ANGPTL2* mRNA than methylation-negative tumors even in this small number of cases. In addition, methylation-negative tumors showed positive ANGPTL2 immunostaining in >10% of cancer cells, whereas methylation-positive tumors showed positive ANGPTL2 staining in <10% of cancer cells, suggesting that methylation is one of the mechanisms suppressing the mRNA and protein expression of ANGPTL2. In neighboring nonneoplastic epithelia, staining for ANGPTL2 was observed (Fig. 3*C*).

Association between expression of ANGPTL2 protein and clinicopathologic characteristics in primary cases. To clarify the clinical significance of ANGPTL2 in OC, the expression level of ANGPTL2 protein in 100 primary OC tissues was evaluated by immunohistochemistry. Negative and positive immunoreactivities of ANGPTL2 (Supplementary Fig. S1) were found in 51 (51%) and 49 (49%) of 100 cases, respectively. The relationship between the expression of ANGPTL2 protein and the clinicopathologic characteristics is summarized in Table 1. In 45 cases from which high-quality DNA was available for a MSP, the methylation status of *ANGPTL2* was inversely correlated with the expression of ANGPTL2 protein ($P = 0.0402$).

ANGPTL2 protein expression in each sample was not associated with age, histologic subtype, tumor staging, the age of patients, the results of surgery, or peritoneal cytology, although data were not fully available for some of those variables. Methylation status in each sample was not associated with these characteristics either (Supplementary Table S4). In overall survival (Fig. 3*D*), no significant difference was observed between the patients with negative and positive ANGPTL2 in all stages. In stage I and II disease, however, negative ANGPTL2 immunoreactivity in tumor cells was significantly associated with a worse overall survival ($P = 0.0432$), whereas positive ANGPTL2 immunoreactivity was significantly associated with a worse overall survival in stage III and IV disease ($P = 0.0039$).

Suppression of cell growth induced by *ANGPTL2* in OC cells. To investigate if restoration of ANGPTL2 expression would suppress the growth of ANGPTL2-nonexpressing OC cells, we performed a colony formation assay using an expression construct of the full-coding sequence of *ANGPTL2* in HNOA, KFr13, and OVSAHO cell lines (Fig. 4*A*). Two weeks after transient transfection and subsequent selection of drug-resistant colonies, the number of larger colonies produced by *ANGPTL2*-transfected cells decreased compared with those of cells transfected with empty vector.

To avoid nonspecific toxicity on OC cells from the forced expression of ANGPTL2, we next assessed the effect of the ANGPTL2 protein treatment on the growth of OC cells. Instead of using purified ANGPTL2, as reported by Zhang and colleagues (18), we used Myc-tagged and His-tagged ANGPTL2 protein–containing conditioned medium prepared from epitope-tagged ANGPTL2 expression vector–transfected SAS cells, which grow in serum-free medium; conditioned medium from mock-transfected cells served as a negative control. The culture supernatant contained secreted

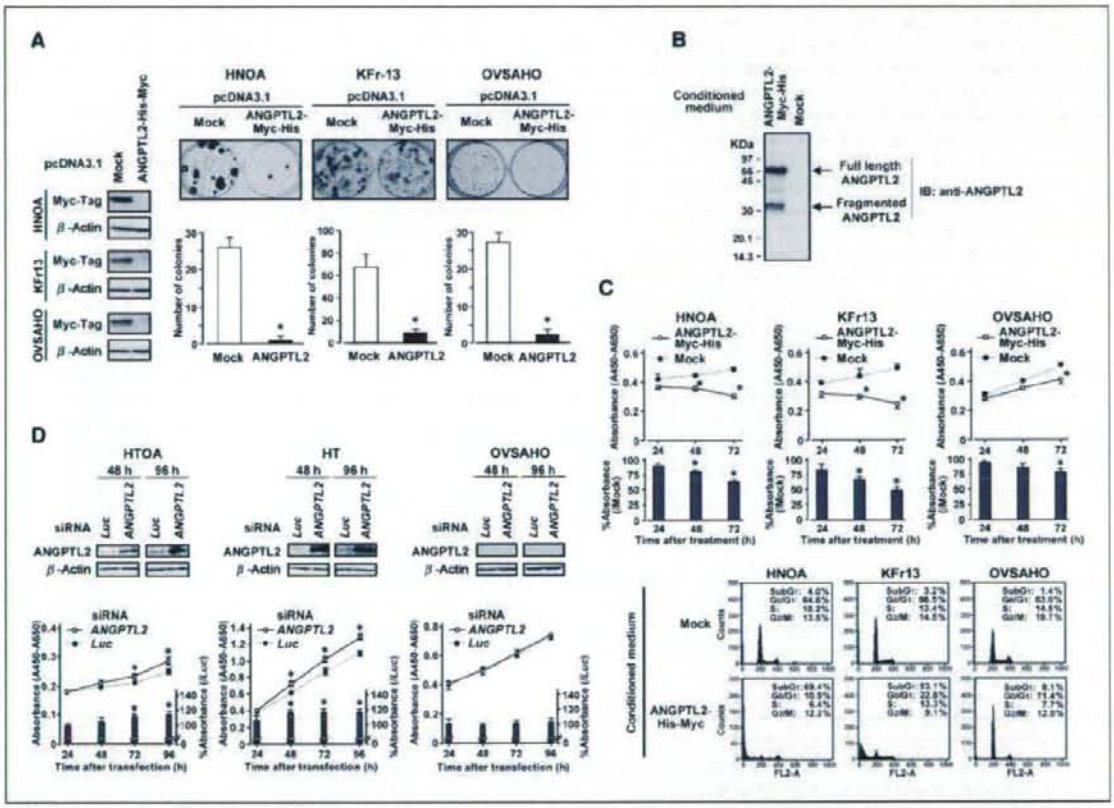

Figure 4. *A*, effects of restoration of ANGPTL2 expression on growth of OC cell lines lacking expression of this gene using colony-formation assay. Cells were transiently transfected with a Myc-tagged and His-tagged construct containing *ANGPTL2* (pcDNA3.1-ANGPTL2-Myc-His), or empty vector (mock), and selected for 2 wk with appropriate concentrations of G418. *Left*, Western blot prepared with 10 μg of protein extract and anti-Myc antibody showing that cells transiently transfected with pcDNA3.1-ANGPTL2-Myc-His expressed Myc-tagged and His-tagged ANGPTL2. *Top right*, 2 wk after transfection and subsequent selection of drug-resistant colonies, the colonies formed by *ANGPTL2*-transfected cells were less numerous than those formed by mock-transfected cells. *Bottom right*, quantitative analysis of colony formation (colonies >2 mm were counted). *Columns*, means of three separate experiments, each performed in triplicate; *bars*, SD (*histogram*). Statistical analysis used the Mann-Whitney *U* test: *, $P < 0.05$. *B*, production of Myc-tagged and His-tagged ANGPTL2 by transfected SAS cells. Western blotting of pooled and concentrated conditioned medium of SAS cells transfected with pcDNA3.1-ANGPTL2-Myc-His encoding Myc-tagged and His-tagged ANGPTL2 (*lane 1*) or pcDNA3.1-mock vector (*lane 2*), probed with ANGPTL2-specific antibody. Two major bands, one at the position expected for Myc-tagged and His-tagged ANGPTL2, and the other a smaller peptide, which may be produced through partial proteolysis (18). *C*, effects of human ANGPTL2 on growth of OC cells. OC cell lines lacking expression of *ANGPTL2* were treated with RPMI 1640 containing 0.2% serum and 1% conditioned medium, which was obtained from the culture of pcDNA3.1-ANGPTL2-Myc-His- or the control pcDNA3.1 mock-transfected SAS cell line lacking expression of ANGPTL2 under serum-free conditions, and concentrated (1:100). *Top*, cell viability was determined by WST assay for 72 h. The percentage of absorbance relative to mock conditioned medium–treated cells at each indicated time (%). *Columns*, means for triplicate experiments, each performed in triplicate; *bars*, SD. Statistical analysis used the Mann-Whitney *U* test: *, $P < 0.05$ vs. control. *Bottom*, representative results of the population in each phase of the cell cycle assessed by FACS 48 h after treatment. A similar result was obtained in the HNOA cell line (data not shown). *D*, effect of knockdown of endogenous ANGPTL2 on growth of OC cells. *ANGPTL2*-specific siRNA (50 nmol/L; *ANGPTL2-siRNA*) or a control siRNA for the luciferase gene (*Luc-siRNA*) was transfected into OC cell lines expressing (*HTOA* and *HT*) or lacking (*OVSAHO*) ANGPTL2, and the number of viable cells after transfection was assessed at the indicated times by WST assay. The percentage of absorbance relative to *Luc*-siRNA–treated cells at each indicated time (%). Western blot confirmed the knockdown of endogenous ANGPTL2 protein expression in HTOA and HT cell lines for 96 h. Because OVSAHO cells lack ANGPTL2 expression through homozygous deletion, its protein expression was not detected. *Columns*, means for triplicate experiments, each performed in triplicate; *bars*, SD. Statistical analysis used the Mann-Whitney *U* test: *, $P < 0.05$ vs. control.

epitope-tagged ANGPTL2 protein migrating with the expected size with some cleaved forms (Fig. 4*B*). Treatment with the conditioned medium containing ANGPTL2 for 72 hours reduced cell viability in the HNOA, KFr13, and OVSAHO cell lines compared with control conditioned medium from mock-transfected cells (Fig. 4*C*, *top*). Upon treatment with conditioned medium containing ANGPTL2, the number of cells decreased with time, most notably, in the HNOA and KFr13 lines. The growth-suppressive effect of conditioned medium containing ANGPTL2 on those OC cell lines decreased by partial but significant depletion of ANGPTL2 (Supplementary Fig. S4). In the FACS analysis of OVSAHO cells, treatment with the conditioned medium containing ANGPTL2 resulted in an accumulation of cells in G_0-G_1 phase but no increase in sub-G_1 phase cells compared with control conditioned medium, whereas in HNOA and KFr13 cells, treatment with the conditioned medium containing ANGPTL2 resulted in an accumulation of cells in sub-G_1 phase (Fig. 4*C*, *bottom*), indicating that ANGPTL2 induced cell death in the HNOA and KFr13 lines, and suggesting that effects of ANGPTL2 on OC cells depend on the cell type, although its receptors and downstream intracellular signaling pathways remain unknown.

To confirm the growth-suppressive effect of ANGPTL2, endogenously expressed ANGPTL2 was knocked down through the introduction of *ANGPTL2*-specific siRNA (*ANGPTL2*-siRNA) into the HTOA and HT cells (Fig. 4*D*). Transfection of *ANGPTL2*-siRNA showed small but significant growth-accelerating effects on those cells compared with that of *Luc*-siRNA, whereas the introduction of *ANGPTL2*-siRNA into OVSAHO cells with a homozygous deletion of *ANGPTL2* had no effect on cell growth compared with that of *Luc*-siRNA, suggesting that the growth-promoting effect of *ANGPTL2*-siRNA on HTOA and HT cells is unlikely to be caused by its nonspecific/off-target effects.

Discussion

In this study, we identified *ANGPTL2* as one of the targets for inactivation in OC from the homozygous loss at 9q33.3, although the possible involvement of other target genes within this region remains unclear. *ANGPTL2* was frequently silenced in OC cell lines through DNA methylation within sequences around the CpG-island exhibiting promoter activity. In primary OCs, lower ANGPTL2 protein levels were frequently observed, and the clinical significance of ANGPTL2 expression might differ among disease stages. In addition, the ectopic expression of ANGPTL2 or treatment with conditioned medium containing ANGPTL2 inhibited the growth of *ANGPTL2*-nonexpressing cells, whereas knockdown of *ANGPTL2* accelerated the growth of *ANGPTL2*-expressing cells, suggesting that ANGPTL2 is likely to work as a functional TSG for OC in a stage-dependent manner.

ANGPTL2 is located at 9q33.3. Although deletion or loss of heterozygosity around 9q33-q34 in OC has been reported previously (19–21), candidates for TSGs within this region have never been identified. The frequent silencing of *ANGPTL2* in cell lines and primary tumors of OC suggests that this gene is one of the targets for 9q33-q34 deletion in this disease. In our array-CGH analysis of 24 cell lines, however, only three lines (12.5%) showed a deletion pattern around *ANGPTL2*: one had a homozygous deletion and two had a hemizygous deletion. In addition, two lines having a hemizygous deletion expressed *ANGPTL2*, suggesting that the silencing of this gene was not simply caused by the deletion of one allele and some other mechanisms, including methylation, in the retained allele. It is possible that additional TSGs other than *ANGPTL2* may exist as targets for deletion around 9q33-q34.

The CpG sites around the *ANGPTL2* CpG-island, whose methylation was associated with the silencing of this gene in some OC cells, showed clear promoter activity. The OC cell lines and immortalized normal ovarian epithelial cell line expressing *ANGPTL2* showed an almost unmethylated pattern around the *ANGPTL2* CpG-island. In addition, demethylation through treatment with 5-aza-dCyd in OC lines with the *ANGPTL2* methylation restored its expression. Therefore, methylation around the *ANGPTL2* CpG-island may contribute to the silencing of this gene. However, some OC cell lines showed reduced *ANGPTL2* expression without DNA methylation, and the effect of 5-aza-dCyd alone on *ANGPTL2* expression was different among those cell lines. In addition, reduced ANGPTL2 protein expression was observed more frequently than *ANGPTL2* methylation in primary OCs, suggesting that epigenetic modifications other than DNA methylation in the *ANGPTL2* gene and/or unknown transcriptional regulatory mechanisms also contribute to the silencing of *ANGPTL2*. Further analyses will be needed to clarify all the mechanisms for ANGPTL2's inactivation and the functional significance of each mechanism in OC.

There are seven known members of the ANGPTL family that share limited sequence homology with angiopoietins (22). Similar to angiopoietins, each ANGPTL protein contains an NH_2-terminal coiled-coil domain and a COOH-terminal fibrinogen-like domain. Unlike angiopoietins, they do not bind to the Tie-2 or Tie-1 receptor (22), and their receptors and downstream signal transduction pathways remain unknown, suggesting that ANGPTLs may have different biological functions than angiopoietins. Although the antigrowth and antimetastatic effects of ANGPTL4 (23, 24), a well characterized member of this family, and DNA methylation of this gene (25) have been reported in some cancers, the expression and methylation status of ANGPTL2 in cancer and their contribution to carcinogenesis have never been previously reported. Although Zhang and colleagues (18) reported very recently that ANGPTL2 and ANGPTL3 stimulate the *ex vivo* expansion of hematopoietic stem cells, their physiologic and pathologic functions remain to be discovered. Notably, we observed clear growth-suppressive effects, such as cell death and G_0-G_1 arrest of ANGPTL2-containing conditioned medium on OC cells, although the effects differed among the OC lines. The growth-suppressive effects of conditioned medium containing His-tagged ANGPTL2 protein significantly decreased after its partial depletion from conditioned medium using Ni-charged resin. These results suggest that (*a*) the growth-suppression of OC cells is not a nonspecific toxic effect of the conditioned medium, and (*b*) the receptors and/or downstream signaling pathways of ANGPTL2 and/or their cross-talk with other signaling pathways, which are still unknown, might differ among cell and/or tissue lineages.

Because the expression status of ANGPTL2 significantly correlates with the survival of patients with OC in a stage-dependent manner, it was suggested that ANGPTL2 shows various biological functions in different stages and functions at least partly as a conditional tumor suppressor for OC. Therefore, the evaluation of the ANGPTL2 expression status with disease stage might be useful for predicting the progression or aggressiveness of this disease, although the question of how tumors in different stages are able to determine the action of ANGPTL2 in carcinogenesis deserves further investigation. We previously showed that CTGF, another bioactive cytokine, also shows conditional tumor-suppressor

activity for OC, although survival analysis in both early and advanced type OC did not reach a level of significance between CTGF-negative and positive cases (11). Because *CTGF* is one of the transcriptional targets for the transforming growth factor-β (TGFβ) signaling pathway, we have speculated that CTGF expression in the advanced stage may be induced by TGFβ in unmethylated tumors (11). It has been suggested that the expression of ANGPTL2 may also be regulated not only by methylation status but also by some upstream signaling pathways, including TGFβ-signaling pathway exerting both tumor-suppressive activity and invasive/metastatic activities through epithelial-mesenchymal transition on epithelial cells, in a progression-dependent manner in OC. Alternatively, receptors and molecules in downstream signaling pathways for ANGPTL2 expressed in tumor cells or other cells, including endothelial cells, might be different among disease stages, resulting in different biological functions in a stage-dependent manner.

Disclosure of Potential Conflicts of Interest

No potential conflicts of interest were disclosed.

Acknowledgments

Received 1/7/2008; revised 3/17/2008; accepted 4/14/2008.

Grant support: Grants-in-aid for Scientific Research on Priority Areas and the 21st Century Center of Excellence Program for Molecular Destruction and Reconstitution of Tooth and Bone from the Ministry of Education, Culture, Sports, Science, and Technology, Japan; the Pancreas Research Foundation of Japan; the Core Research for Evolutional Science and Technology of Japan Science and Technology Corporation; and the New Energy and Industrial Technology Development Organization.

The costs of publication of this article were defrayed in part by the payment of page charges. This article must therefore be hereby marked *advertisement* in accordance with 18 U.S.C. Section 1734 solely to indicate this fact.

We are grateful to Dr. Hidetaka Katabuchi (Kumamoto University School of Medicine) for providing the OSE-2a cell line, and Ayako Takahashi and Rumi Mori for technical assistance.

References

1. Cannistra SA. Cancer of the ovary. N Engl J Med 2004;351:2519–29.
2. Jemal A, Siegel R, Ward E, Murray T, Xu J, Thun MJ. Cancer Statistics, 2007. CA Cancer J Clin 2007;57:43–66.
3. Ozols RF, Bookman MA, Connolly DC, et al. Focus on epithelial ovarian cancer. Cancer Cell 2004;5:19–24.
4. Prowse A, Frolov A, Godwin AK. The genetics of ovarian cancer. In: Ozols RF, editor. American Cancer Society Atlas of Clinical Oncology. Hamilton (Ontario): B.C. Decker Inc.; 2003. p. 49–82.
5. Inazawa J, Inoue J, Imoto I. Comparative genomic hybridization (CGH)-arrays pave the way for identification of novel cancer-related genes. Cancer Sci 2004;95:559–63.
6. Friend SH, Bernards R, Rogeli S, et al. A human DNA segment with properties of the gene that predisposes to retinoblastoma and osteosarcoma. Nature 1986;323:643–6.
7. Kamb A, Gruis NA, Weaver-Feldhaus J, et al. A cell cycle regulator potentially involved in genesis of many tumor types. Science 1994;264:436–40.
8. Hahn SA, Schutte M, Hoque AT, et al. DPC4, a candidate tumor suppressor gene at human chromosome 18q21.1. Science 1996;271:350–3.
9. Li J, Yen C, Liaw D, et al. PTEN, a putative protein tyrosine phosphatase gene mutated in human brain, breast, and prostate cancer. Science 1997;275:1943–7.
10. Jones PA, Baylin SB. The fundamental role of epigenetic events in cancer. Nat Rev Genet 2002;3:415–28.
11. Kikuchi R, Tsuda H, Kanai Y, et al. Promoter hypermethylation contributes to frequent inactivation of a putative conditional tumor suppressor gene connective tissue growth factor in ovarian cancer. Cancer Res 2007;67:7095–105.
12. Takada H, Imoto I, Tsuda H, et al. ADAM23, a possible tumor suppressor gene, is frequently silenced in gastric cancers by homozygous deletion or aberrant promoter hypermethylation. Oncogene 2005;24:8051–60.
13. Imoto I, Izumi H, Yokoi S, et al. Frequent silencing of the candidate tumor suppressor PCDH20 by epigenetic mechanism in non-small-cell lung cancers. Cancer Res 2006;66:4617–26.
14. Takada H, Imoto I, Tsuda H, et al. Genomic loss and epigenetic silencing of very low density lipoprotein receptor involved in gastric carcinogenesis. Oncogene 2006;25:6554–62.
15. Nitta M, Katabuchi H, Ohtake H, Tashiro H, Yamaizumi M, Okamura H. Characterization and tumorigenicity of human ovarian surface epithelial cells immortalized by SV40 large T antigen. Gynecol Oncol 2001;81:10–7.
16. Suzuki E, Imoto I, Pimkhaokham A, et al. PRTFDC1, a possible tumor-suppressor gene, is frequently silenced in oral squamous-cell carcinomas by aberrant promoter hypermethylation. Oncogene 2007;26:7921–32.
17. Xiong Z, Laird PW. COBRA: a sensitive and quantitative DNA methylation assay. Nucleic Acids Res 1997;25:2532–4.
18. Zhang CC, Kaba M, Ge G, et al. Angiopoietin-like proteins stimulate *ex vivo* expansion of hematopoietic stem cells. Nat Med 2006;12:240–5.
19. Schultz DC, Vanderveer L, Buetow KH, et al. Characterization of chromosome 9 in human ovarian neoplasia identifies frequent genetic imbalance on 9q and rare alterations involving 9p, including CDKN2. Cancer Res 1995;55:2150–7.
20. Devlin J, Elder PA, Gabra H, Steel CM, Knowles MA. High frequency of chromosome 9 deletion in ovarian cancer: evidence for three tumour-suppressor loci. Br J Cancer 1996;73:420–3.
21. Sonoda G, Palazzo J, du Manoir S, et al. Comparative genomic hybridization detects frequent overrepresentation of chromosomal material from 3q26, 8q24, and 20q13 in human ovarian carcinomas. Genes Chromosomes Cancer 1997;20:320–8.
22. Oike Y, Yasunaga K, Suda, T. Angiopoietin-related/angiopoietin-like proteins regulate angiogenesis. Int J Hematol 2004;80:21–8.
23. Li KQ, Li WL, Peng SY, Shi XY, Tang HL, Liu YB. Anti-tumor effect of recombinant retroviral vector-mediated human ANGPTL4 gene transfection. Chin Med J (Engl) 2004;117:1364–9.
24. Galaup A, Cazes A, Le Jan S, et al. Angiopoietin-like 4 prevents metastasis through inhibition of vascular permeability and tumor cell motility and invasiveness. Proc Natl Acad Sci U S A 2006;103:18721–6.
25. Kaneda A, Kaminishi M, Yanagihara K, Sugimura T, Ushijima T. Identification of silencing of nine genes in human gastric cancers. Cancer Res 2002;62:6645–50.

Clinical Translational Research

Oncology

Oncology 2008;75:32–41
DOI: 10.1159/000151667

Received: December 27, 2007
Accepted after revision: April 15, 2008
Published online: August 26, 2008

A New Formula for Predicting Liver Metastasis in Patients with Colorectal Cancer: Immunohistochemical Analysis of a Large Series of 439 Surgically Resected Cases

Hiroki Ochiai[a, e] Yukihiro Nakanishi[a] Yuri Fukasawa[a] Yasunori Sato[b] Kimio Yoshimura[b] Yoshihiro Moriya[c] Yae Kanai[a] Masahiko Watanabe[f] Hirotoshi Hasegawa[e] Yuko Kitagawa[e] Masaki Kitajima[d] Setsuo Hirohashi[a]

Divisions of [a]Pathology, [b]Genetics and [c]Surgery, National Cancer Center Research Institute and Hospital, and [d]International Health and Welfare University, [e]Department of Surgery, Keio University School of Medicine, Tokyo, and [f]Department of Surgery, Kitasato University School of Medicine, Kanagawa, Japan

Key Words
Clinicopathological study · Colorectal cancer · Dysadherin · E-cadherin · Liver metastasis · Matrilysin

Abstract
Objective: The purpose of this study was to establish a new formula predicting liver metastasis in patients with colorectal cancer (CRC). ***Methods:*** Nine previously reported predictive markers for liver metastasis and/or prognosis (COX-2, dysadherin, E-cadherin, β-catenin, Ki-67, p53, laminin5-γ2, matrilysin and MUC-1) were immunohistochemically investigated in 439 consecutive patients with CRC. We tried to determine the combination of molecules which best predicted liver metastasis. A formula for predicting liver metastasis was constructed using a training cohort comprising 150 cases, and applied to a validation cohort comprising 190 cases and another comprising 99 cases from an outside hospital. ***Results:*** A combination of dysadherin, E-cadherin and matrilysin was identified to be best for predicting liver metastasis (area under the curve value, 0.807). The predictive formula: 3× dysadherin score [0 for low expression (≤50% of tumor cells positive) or 1 for high expression (>50%)] + 4× E-cadherin score [0 for preserved (>80% of tumor cells positive) or 1 for reduced (≤80%)] + 2× matrilysin score [0 for low expression (≤30% of tumor cells positive) or 1 for high expression (>30%)] was able to discriminate patients with liver metastasis in the training cohort with a sensitivity of 85.7% and a specificity of 58.9%. The discriminative capacity of the formula was validated in the first cohort with a sensitivity of 87.0% and a specificity of 66.5%, and in the second cohort with a sensitivity of 80% and a specificity of 60.0%. ***Conclusions:*** We have established a formula for predicting liver metastasis in patients with CRC, and confirmed that it has a high sensitivity potentially useful for clinical application.

Y.S. is presently at the Department of Biostatics, Harvard School of Public Health, Boston, Mass., USA.

KARGER
Fax +41 61 306 12 34
E-Mail karger@karger.ch
www.karger.com

0030–2414/08/0752–0032$24.50/0

Accessible online at:
www.karger.com/ocl

Setsuo Hirohashi, MD
Division of Pathology, National Cancer Center Research Institute
5-1-1 Tsukiji, Chuo-ku
Tokyo 104-0045 (Japan)
Tel. +81 3 3542 2511, ext. 4101, Fax +81 3 3248 2463, E-Mail shirohas@ncc.go.jp

Introduction

Colorectal cancer (CRC) is the third most common malignant tumor in the world [1]. Its prognosis after curative resection depends exclusively on the development of metachronous metastases, especially liver metastasis [1]. To improve the prognosis of CRC, the most important considerations are the selection of patients at high risk for liver metastasis and subsequently the institution of appropriate adjuvant therapy. Adjuvant therapy in patients with CRC after curative resection has been reported to be useful for improving overall and disease-free survival [2–4]. Resection of liver metastases offers a chance for prolonged survival [5, 6]. Patients with intermediate-stage disease (stage II or III) have a recurrence rate of about 20–50%, including liver and lung metastases, recurrence in lymph nodes and peritoneal dissemination [2, 3, 7]. The remaining 50–80% have no recurrence, and therefore these patients underwent unnecessary adjuvant chemotherapy. To increase the survival benefit from adjuvant chemotherapy and the early detection rate of surgically resectable liver metastasis, the selection of patients at high risk for liver metastasis is essential.

Conventional risk factors for liver metastasis include lymph node metastasis, venous, serosal and lymphatic invasion, tumor dedifferentiation, white streak sign and resection margin [1, 8–14]. The accuracy of diagnosing liver metastasis using these conventional markers has been reported to be between 24 and 98% in terms of sensitivity, and between 34 and 97% in terms of specificity [1, 8–13]. Recently, many molecular markers have been reported to be useful for predicting liver metastasis and thus prognosis in CRC patients [15–19]. Therefore, in the present study, we tried to determine the best combination of the immunohistochemically detectable molecules already reported for predicting liver metastasis, and to establish a new formula for accurate prediction of liver metastasis in CRC patients.

Materials and Methods

Patients and Samples

Four hundred thirty-nine patients with CRC were selected from the lists of patients treated at the National Cancer Center Hospital (Tokyo, Japan) between 1995 and 1998 and the Kitasato University (Kanagawa, Japan) between 2000 and 2002. The patients included 267 (60.8%) men and 172 (39.2%) women, ranging in age from 21 to 93 years (median 62 years). Sample selection was restricted to consecutive cases diagnosed as stage II (44.2%, 194 of 439) or III (55.8%, 245 of 439). All patients had undergone curative resection. None of the patients had received chemotherapy or radiotherapy preoperatively. Follow-up studies were complete in all patients, ranging from 0.1 to 8.3 years (median, 5.5 years). Two patients who were followed up for 0.1 months died of pulmonary embolism 3 and 4 days after surgery, respectively. Recurrence after surgery was diagnosed by ultrasonography, computed tomography and angiography. Tumor location, lymph node, liver and lung metastases, tumor size, and lymphatic and venous invasion were all classified according to the TNM classification [20]. Histologically, tumors were classified according to the International Histological Classification of Tumors of the World Health Organization [21]. Among the study cases, 188 (42.8%) were classified as well-differentiated adenocarcinomas, 231 (52.6%) as moderately differentiated, 11 (2.5%) as poorly differentiated, 6 (1.37%) as mucinous and 2 (0.46%) as signet-ring-cell adenocarcinomas. During the follow-up period, liver metastases were observed in 49 (11.2%) cases, and at the time of writing this has proved fatal in 28 (57.2%) cases.

We divided the 439 patients into three groups. Group I included 150 consecutive patients, 94 men (62.7%) and 56 women (37.3%), ranging in age from 21 to 87 years (median, 63 years), operated on at the National Cancer Center Hospital between January 1, 1995, and July 1, 1996. In group I, 21 patients (14%) developed liver metastases and were used as a training cohort. Group II included 190 consecutive patients, 116 men (61.1%) and 74 women (38.9%), ranging in age from 32 to 93 years (median, 62 years), who were operated on at the National Cancer Center Hospital between July 1, 1996, and January 1, 1998. In group II, 24 patients (12.6%) developed liver metastases; they were used as the first validation cohort. Group III included 99 consecutive patients, 57 men (57.6%) and 42 women (42.4%), ranging in age from 27 to 85 years (median, 62 years), who were operated on at the Kitasato University between January 1, 2000, and January 1, 2003. In group III, 5 patients (5.1%) developed liver metastases; they were used as the second validation cohort.

Search Strategy and Selection Criteria for Antibodies

We selected nine previously reported molecules for immunohistochemical study – β-catenin [22–26], cyclooxygenase-2 (COX-2) [16, 27, 28], dysadherin [18, 29–31], E-cadherin [18, 23, 32], Ki-67 [33, 34], p53 [11, 34–36], matrilysin [37, 38], MUC-1 [19, 33] and laminin5γ2 [17, 39, 40] – as the prognostic significance of the expression of these markers has already been reported in several papers in which multivariate logistic regression analysis was performed, and reliable figures and descriptions of immunostaining were demonstrated (table 1).

Immunohistochemistry

Resected primary colon cancers were cross-sectioned in order to obtain tissue sections according to the general rules for clinical and pathological studies on cancer of the colon, rectum and anus [41]. Representative tissue sections taken at the maximum cross-section, each containing the deepest site of cancer invasion, were subjected to immunohistochemical staining using the avidin-biotin peroxidase complex method [42]. After deparaffinization in xylene and rehydration in ethanol, the sections were heated in citrate buffer (10 mM, pH 6.0) at 120°C for 10 min for antigen retrieval. Endogenous peroxidase was blocked with 0.3% hydrogen peroxidase in methanol for 20 min. The sections were then incubated with anti-dysadherin antibody (M53; 1:500 dilution, established in our laboratory [31]), anti-E-cadherin antibody (HECD-